Detecting high spatial variability of ice-shelf basal mass balance (Roi Baudouin ice shelf, Antarctica) S. Berger et al – TCD 2017 – doi:10.5194/tc-2017-41

Here we respond point-by-point to the 2 reviews and the interactive comment. We found that the overall feedback is positive and constructive. We thank the referees David Shean and Geir Moholdt for their time and respond to their comments below. The main changes in the revised manuscript include:

- Reordering of the figures, addition of new Figures 1 and 9 and considerable modifications in new Figures 3 and 5.
- Inclusion of three supplementary Figures
- A more detailed accuracy assessment of the TanDEM-X DEMs
- The reorganisation of section 2 (data and methods) and 4 (Error sources). The former has been changed to better explain the calibration and matching of the different DEMs while the latter is reorganised to better emphasise our accuracy analysis of DEMs

In Eqs 1 and 2 we have replaced H with H_i to state more clearly that the thickness is computed and considered in ice-equivalent units. The main conclusions of the paper remain unaltered.

Our replies are printed in blue and numbered as G1.x and G2.x for general comments from reviewers 1 and 2, respectively. Specific comments are referred to with page and line numbers used by the reviewers.

Sophie Berger, Laboratoire de Glaciologie, Université Libre de Bruxelles, Belgium

Response to Reviewer 1 (David Shean)

Summary

This paper documents the high-resolution basal mass balance for the Roi Baudouin ice shelf for 2013-2014 using TanDEM-X DEMs. The authors provide a good description of the Lagrangian basal mass balance derivation (building on previous literature for analyses of other ice shelves), and compare DEM-derived basal mass balance with in situ pRES data and GPS-derived basal mass balance. In general, the methodology, results, and figures are well done. There are several issues that require further attention before publication. The authors claim to use a novel method to improve quality of velocity divergence products. The resulting products still contain fairly significant noise and the authors provide only one comparison with a coarse smoothing approach which generally looks similar. There are some significant discrepancies between firn air content from a dynamic firn densification model (RACMO-FDM) and the in situ radar data, with different assessments of significance. The authors offer a detailed analysis of an ice-shelf surface depression, which they interpret as a moving, unfrozen englacial lake 30 m below the surface. There is limited evidence to support this speculative interpretation. The LBMB derived from pRES/GPS measurements shows some significant differences when compared to the DEM derived LBMB. On the whole, this is a good paper that should be published after these and other issues are addressed.

We appreciate your detailed comments and have included many of them in the revised version. We first address the general comments before dealing with specific ones.

General comments

G1.1: The authors claim to use a novel method to improve quality of velocity divergence products. The resulting products still contain fairly significant noise and the authors provide only one comparison with a coarse smoothing approach which generally looks similar.

We agree that the initial version did not sufficiently discuss the differences between smoothing and total-variation regularization. Our initial motivation for using the latter was that it treats jump discontinuities more accurately than the corresponding smoothing approaches (Chartrand, 2011). This is important, because we suspect that ice-flow velocities change abruptly in ice-shelf channels that experience strong basal melting (Drews, 2015).

We now compare the regularized velocity divergence (with a fixed alpha given by the estimated variance in the velocity data), with divergences derived from velocity fields that have been smoothed to a varying degrees (average filter with kernel dimensions varying from 375x375 m to 1,875x1,875 m). The results are displayed in the new Fig 3. We find that the regularized derivative shows the strongest ice-flow divergence across an ice-shelf channel. Outside the ice-shelf channel, the regularized derivative is smoother than the derivative resulting from the 375x375 m smoothing, which is the only velocity field with a comparable divergence in the channel's surface depression. This shows that smoothing and regularization are not equivalent in detecting small-scale velocity anomalies around ice-shelf channels. However, for the Roi Baudouin Ice Shelf overall differences between regularizing and smoothing are relatively minor and the resulting LBMB estimates barely differ (because the correction for ice-flow divergence is small). This may not be the case for other ice shelves.

Figure 3 (new) has now been updated and we state this analysis now more clearly in the revised version.

G1.2 : There are some significant discrepancies between firn air content from a dynamic firn densification model (RACMO-FDM) and the in situ radar data, with different assessments of significance.
It is correct that RACMO-FDM does not correctly resolve the wind-albedo feedback close the grounding line. Consequently, the observed blue-ice area is not adequately represented in the modelled firn-air content. The impact of this misestimation on the derivation of the hydrostatic ice thickness has been discussed by Lenaerts et al. (2017). We reference this discussion in the revised version and mention the correspondingly increased uncertainty in the LBMB rates in those areas.

G1.3 : the authors offer a detailed analysis of an ice-shelf surface depression, which they interpret as a moving, unfrozen englacial lake 30 m below the surface. There is limited evidence to support this speculative interpretation.
Lenaerts et al (2017) witnessed subsurface meltwater features, such as the englacial lake shown below on the Roi Baudouin Ice Shelf. Using satellite data they identify 55 other and potentially refrozen englacial lakes on the ice shelf. The elliptical depression is one of them.

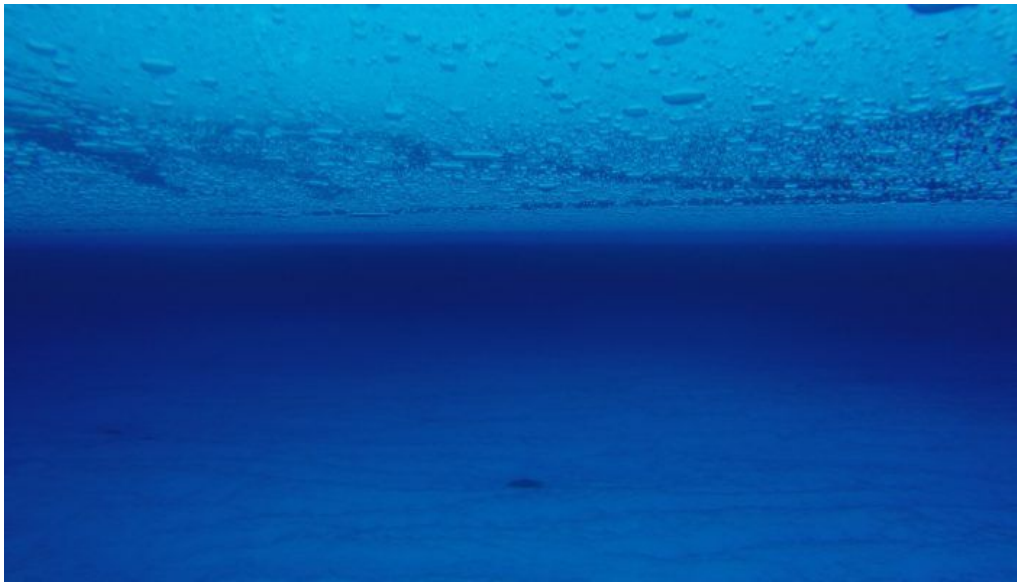

It is correct that we have no direct evidence for liquid water beneath the elliptical surface depression. It is now more clearly stated in the text, that if the elliptical depression once formed an englacial lake, it has probably refrozen by now and that the refrozen interface could block radar penetration.

This is now clarified in the text. We now only mention the englacial lake found farther upstream. The feature farther downstream is now referred to exclusively as an "elliptical surface depression" clearly marking that the origin of this feature is not fully known .

G1.4 : The LBMB derived from pRES/GPS measurements shows some significant differences when compared to the DEM derived LBMB.
We agree that the term near-perfect is too strong. However, given that estimated error of the LBMB is easily with a few meters per year we were surprised to see such little deviation on the eastern side

of the elliptical surface depression. The deviations on the western (i.e. left) side are certainly more significant and maybe linked to a more complex topography (finger-like features). We adapted the wording for comparing the pRES data with the LBMB accordingly.

G1.5: abstract ending

The abstract ends with a mention of challenges for full coupling between ice and ocean models, but this is never addressed in the paper.

Thanks for pointing this out. We find it not uncommon to end the abstract with a phrase stating the wider context, even though this context is not fully explored. To substantiate this point, we added a sentence in section 5 "Second, this sub-kilometre variability in ice-ocean processes poses challenges for coupling ice with ocean models, because highly resolved oceanic models have a typical resolution of 1-2 km (Dinniman et al, 2016), and community efforts such as the Marine Ice Sheet–Ocean Model Intercomparison Project prescribe horizontal gridding of 2 km (Asay-Davis et al, 2016). This is too coarse to fully capture the spatial variability that we observe here."

G1.6 : structure of the method section

Methods section needs some reorganization. Recommend separating DEM generation from hydrostatic ice thickness calculation. Agreed. We have now reorganized the old section "Hydrostatic ice thickness" (2.4-old) into two subsections "surface elevations" and "hydrostatic equilibrium" (not numbered). Moreover, we have added a new section "Lagrangian thickness change" (2.5-new). Here, we now explain the matching procedure in greater details.

G1.7 : Analysis of TanDEM-X accuracy

No meaningful analysis of TDM DEM accuracy is provided, only "estimated relative vertical accuracy better than 1 m (based on the standard deviation in overlapping areas)" – where are these areas? Are they all flat, or does this include higher surface slopes (like the surface depressions over channels discussed in the text)? Are you certain these areas are not evolving during the 2013-2014 period due to SMB or dynamics? A much more convincing approach would be to show a figure of DEM standard deviation over static surfaces (exposed bedrock, slow-moving ice with limited SMB).

Agreed. In the revised version we now address the DEM accuracy in the new subsection "Calibration and accuracy of TanDEM-X elevations" of section 4.1. To do so, we are using the following techniques:

1. Fig. S3 (Supplements) now shows the difference maps between overlapping individual frames from the same day, after calibration with a constant offset and Gaussian filtering but prior to the plane fitting. As detailed in the text, the offset accounts for unknown offsets from phase unwrapping, tidal uplift, inverse barometer effect, and for the spatially averaged depth penetration of the TanDEM-X signal. The applied offset correction is typically less than a few meters. Difference maps in new Fig. S3 show a discrepancy of 0.0+/-0.3 m with a slight spatial trend. We attribute these trends to residual phase ramps occurring during the bistatic processing of the TanDEM-X data. This bias typically ranges from -0.2 to 0.2 m except for the two northernmost difference fields which exhibit trends from -0.8 to 0.8 m. We correct these trends with plane fitting of 2014 to 2013 frames (Sect 2.4). In addition to the systematic bias, discrepancies with a magnitude of 0.5 m occur in steep areas (e.g ice-shelf channels or surface ridges).

2. New Fig. 9 compares the 2013 and 2014 TanDEM-X mosaics with two GNSS profiles.

- The mosaic from August and October 2013 is compared with a kinematic 20 x 25 km GNSS survey collected in December 2012. The investigated area includes strong topographic changes due to ice-shelf channels and a pinning point. The observed discrepancy is -0.44 +/- 1.05 m. Differences are largest inside ice-shelf channels because of dynamic topographic changes due to ice advection in the 8-10 month time interval between

GNSS surveying and DEM acquisition. Excluding these areas lowers the discrepancy to -0.37+/-0.29 m .

- The mosaic from June and July 2014 deviates with -0.04+/-0.65 m from a 100 km GNSS transect collected in December 2014. Similar to above, differences are largest in ice-shelf channels (i.e. the advection of an ice-shelf channel junction within the 6-7 month interval) and they lower to -0.07+/-0.55 m when ice-shelf channels are excluded from the comparison.

  Apart from the channel, whose dynamic influence smear out other potential biases (changing SMB, variable penetration depth), we find the largest discrepancy close to the grounding line. There, the TanDEM-X elevations are overestimated by up to 2 m. This is discussed in reply G1.8.

The straightforward approach to evaluate our DEM at rock outcrops, or areas of zero SMB, is not possible because such areas do not exist in our area of interest. (Rock outcrops are extremely rare in all of the coastal Dronning Maud Land areas). Due to offset correction and plane fitting, we have to assume that the overall $\partial Hi / \partial t$ is zero.

All these points are now included in the revised manuscript in Section 4.1 and Fig S3 (supplementary) and Fig. 9

G1.8 : Penetration of radar

Are you convinced that you are not seeing penetration of the radar into snow and ice in the TandDEM-X DEMs? Other studies have shown this can be several meters, potentially up to 10 meters in cold, dry snow. This could impact the comparisons with GNSS surface elevations.

Thanks for pointing this out. Humbert and Steinhage (2011) estimated that the TerraSAR-X signal penetrates in to the dry snow of the Fimbul Ice shelf by 8-10 m. In our case, the bulk part of such a signal penetration would be accounted for during the offset correction of the DEMs. However, a spatially or temporally varying signal penetration would result in a bias of our LBMB estimates.

In our area of interest, we would expect the largest spatial gradient in signal penetration in the North-South direction, where the depth of the firn column changes from about 15 m (firn-air content) near the ice-shelf edge, to 0 m in the blue ice belt close to the grounding line. As explained in the previous reply (G1.7), the TanDEM-X DEM in this area is systematically higher by about 2 m. This may be a relict of a variable signal penetration from the TanDEM-X satellites.

We discuss this point now more clearly (section 4.1) , although we do not have the means to fully resolve it.

G1.9 : combination of TanDEM-X frames

No dates (month, day) are provided for the TDM DEMs, and we don't know over what period the "32 from 2013" and "11 from 2014" actually cover. Agreed. Figure S1 (supplementary) now shows the location of the different TanDEM-X frames and their acquisition date. In addition, section 2.4 has been rephrased to "The processing provides 43 single DEMs (32 from 2013 and 11 from 2014) gridded to 10 m. They cover a time span ranging from 21/06/2013 to 10/07/2014 (Fig. S1 – supplementary). The maximum time difference at overlapping areas between the 2013 and 2014 DEMs is 379 days."

Were mosaics generated for each year, centred on Jan 1 of the respective year? Did you compute Lagrangian Dh/Dt for each pair of DEMs, or for the annual mosaics? The only DEMs that are mosaicked and treated as one piece are the different frames acquired on the same day and from the same satellite path. The Lagrangian DH/Dt was computed for each pair of overlapping DEMs, meaning that the time difference (Dt) varies from one pair to another. This was taken into account when calculating the corresponding melt rates in meters per year.

What about offsets between DEMs within a single year – if they are months apart, won't there be significant advection for areas flowing 300 m/yr? As we shift the 2013 DEMs forward, the Lagrangian framework reflects the 2014 geometry. And, as shown in Fig. S1 (supplementary), the 2014 DEMs span from 07/06/2014 to 10/07/2014, with a maximum time difference of 33 days between two overlapping DEMs of the same year. Even in areas flowing 300 m/a, this coincides with a shift of only 3 pixels (compared to a shift of 30 pixels after a year).

G1.10: Gaussian filter

The authors indicate that they smoothed their input 10-m posting TanDEM-X DEMs with a gaussian filter (no filter dimensions provided, but 7-sigma implies a large kernel). This inherently reduces the resolution of these DEMs, and will smooth edges of small-scale features like channels.
The Gaussian filter we chose has a standard deviation/coverage of 7 pixels (or 70 m) in either direction. This means that points lying within that distance are weighted with 0.68. At 14 pixels distance (or a radius of 140 m) the weight increases to 0.95.
The size of the Gaussian filter is chosen based on a comparison with a GNSS transect collected in 2012. We investigated standard deviations/coverages from 1-10 pixels and found that using 7 pixels minimises the standard deviation between GNSS and TanDEM-X surface elevation. As shown in Figure S2 (supplements) the applied smoothing does not affect the shape of the surface depressions linked to ice-shelf channels (with a typical width of 1-2 km).

G1.11: It is important to be clear that the DEMs are measuring surface elevation and the surface expression of features interpreted as basal channels. You are not directly measuring channel depth using surface elevation. Agreed. we have changed the text accordingly.

G1.12: Are there any airborne radar profiles (OIB, BAS, etc.) over this shelf? Seems like there must be something available. If so, you can use observed ice thickness and deviation from floatation thickness calculated from your surface elevations to estimate firn air content [Holland et al., 2011]. Our analysis around the elliptical surface depression includes a comparison between the hydrostatic ice thickness with ground-based radar. We infer a theoretical firn-air content (assuming hydrostatic equilibrium and absence of marine ice) which corresponds to the approach of Holland et al. (2011). There are no other airborne profiles in this area which could be used to do this analysis on a larger scale. (OIB has not surveyed this sector of Antarctica yet, and other airborne profiles have focused on gravimetry requiring a large flight height deteriorating the radar data).

G1.13: The ordering of the figures is a bit odd – the comparison showing divergence for regularization vs. smoothed velocities should be shown after describing the method, or early in the results. The LBMB figure (the main result) should come after the component figure. We rearranged the Figure order, also based on suggestions from Reviewer 2. Figure 1 is now a new figure that locates the on-site datasets.

Specific comments (and additional general comments that came up for specific sections)

Page 1:
Line 12: Is the lake 30 m or the surface depression is 30 m below surrounding surfaces? We deduced from the radar profile that the upper surface of the characteristic radar reflector lies approximately 30 m below the surface. However, the depression is 10 m lower that the surrounding., and this is the value that we now mention in the abstract.
Lines 16-17: see reply G1.5
Line 21: Not sure "Marine Ice Sheet Instability" should be capitalized, changed to 'marine ice sheet instability'

Page 2:
Line 10: delete "the" before "the BMB" We are not sure about the correct usage here and will keep

an eye on it during typesetting.
Line 11: “which form” done
Line 11-12: I don’t understand this 50% claim, also, the sentence ends abruptly – missing “surrounding ice”? We have changed this sentence to make it more understandable: “Ice-shelf channels are one expression of localised basal melting (Stanton et al, 2013,Marsh et al 2016) which, due to hydrostatic adjustment, form curvilinear depressions visible at the ice-shelf surface (Fig. 1). These surface depressions virtually always reflect basal incisions resulting in curvilinear tracts of thin ice. In some areas, ice-shelf channels are twice as thin as their surroundings (Drews, 2015)”. Note that an ‘s’ was missing in surroundings.
Line 10: What about GPS receivers [Jenkins et al., 2006; Shean et al., 2017]? Reference to Shean et al (2017) has been added.
Line 14: Channel carving does not cause increased crevassing – these are separate processes. The link between ice-shelf channel formation and basal crevassing has been proposed by Vaughan et al (2012) (see figure below).

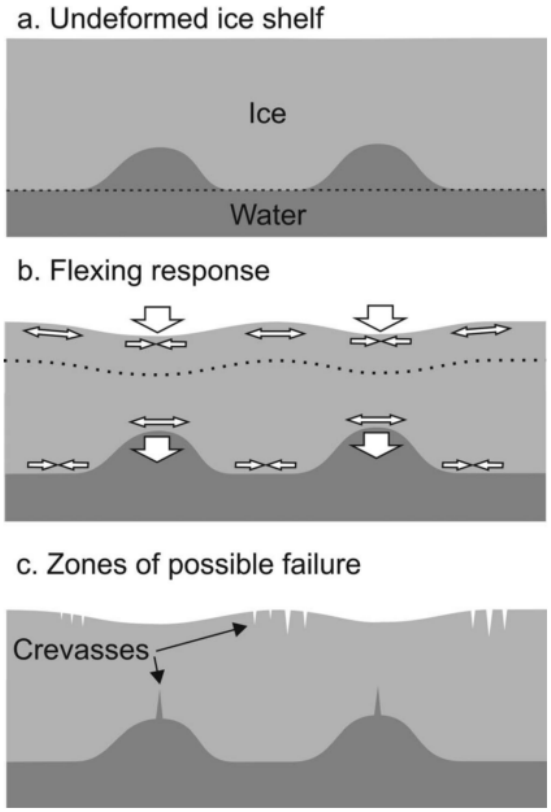

Figure 6. Drawing of the formation of surface and basal crevasses based on thin-beam theory.

Line 16: delete “at 10 m gridding” – not relevant for intro Thank you for your suggestion but we would like to keep this part, as the spatial resolution is important for the paper.
Line 17 and later: I believe TC should be “Figure” not “Fig.” Journal guidelines require using “Fig.” unless at the beginning of a sentence where “Figure” should be used. We have adapted our notation accordingly.
Line 22: delete “all the way” done
Line 23: delete “In the following,” done
Line 24: delete “results”, also suggest “with focus on…” rather than “special focus” done
Line 26-28: “accounts for” is a bit awkward – you are mitigating the noise, not accounting for it agreed. Changed to “mitigates the noise”
Line 29: change “observational evidence” to “observations” done
Line 29: suggest simplifying to “…validated with phase-sensitive radar, ground-penetrating radar, and GNSS observations.” done, we have rephrased your suggestion “validated with phase-

sensitive radar, GNSS observations and ground-penetrating radar."

Page 3:
Equation 1: This is 3 equations! Should probably split. You might start with the standard mass conservation rather than rearranging at the start. Thanks for the suggestion. The three lines are now referred to as sub-equations (1a), (1b) and (1c) .
Line 6: "vertically integrated" (no hyphen needed) – perhaps "column-average" is a better descriptor here. You are assuming surface velocity is equal to column-average velocity, this should be stated somewhere. Agreed. Changed to "the column-average horizontal velocity of the ice". We also added this at the beginning of section 2.2 (surface velocities from satellite radar remote sensing) : "Assuming that that velocities do not vary with depth….. "
Line 6: "In principle, " done

Page 4
Line 1: Not sure what you mean here - Eulerian dH/dt involves two thickness measurements. What we mean is that usually studies using an Eulerian framework only rely on 1 thickness field and an external dataset for the thickness change, instead of computing it from two different thickness fields. We have now rephrased that part: "Eulerian studies are often based one thickness field and either assume steady-state (Rignot and Steffen, 2008; Neckel et al 2012) or rely on an external dataset (Depoorter et al, 2013, Rignot et al, 2013) to account for the thickness changes $\partial Hi / \partial t$ (e.g. Pritchard et al, 2012; Paolo et al 2015) " .
Line 6: "can only be adequately done" is subjective. Agreed. Changed to "The Lagrangian approach is best-suited in areas where advection is significant (e.g. near ice-shelf channels)."
Line 7: Add [Shean, 2016; Shean et al., 2017] for additional derivation and discussion of Eul/Lag elevation change. Shean et al, 2017 added. Unfortunately we do not have access to the PhD thesis Shean (2016).

Line 10: "from 2013 and 2014" done
Line 10: Suggest deleting ", clearly resolving ice-shelf channels" – you are claiming that the 10-m resolution is novel (a claim some might reject). This resolution can resolve many small-scale features on ice shelves, not just channels. OK, removed.
Why so many details in paragraph 2? Details like "we calculate Lag thickness change by crosscorrelating the TanDEM-X DEMs (using 5x5 km2 patches…) should be in Section 2.5. Agreed. We have added a new subsection "Lagrangian thickness change" (2.5-new) (see response G1.6)
5x5 km2 – I think you mean 5 km x 5 km. yes changed.
OK, so you have 10-m DEMs, and you are cross-correlating using a 500x500 pixel kernel. Using a kernel this large inherently reduces the resolution of the output velocity products. Did you do this for every pixel, or for some sparse interval? We think we did not explain this part very well: the velocity field is not a product from the DEM matching. Instead we matched the DEMs and then used an external velocity field of the area (from Berger et al 2016). We matched DEM patches of 5x5 km sampled every km (to make sure to the shifting covers every area). This is now better explained in the new section "Lagrangian thickness change" (2.5-new).

Line 17: "freely floating" Sorry we don't understand that comment.
"viscous inflow in ice-shelf channels" is a process, not a "small-scale feature" Ok, we rephrased the sentence "...but also other small-scale features such as ice-shelf channels where viscous inflow can occur ..."

Line 24: "of 1996" and "of 2010" should be "from 1996" done
Line 24-25: So, you compared the 1996, 2010 and 2014 velocities and found no evidence for temporal variations? What are dates of the input InSAR? What was time period of GNSS? Surely

the velocities aren't identical. The remote sensing flow field is a mix of InSAR velocities from 1996 and speckle tracking from 2010 (see table below from Berger et al (2016), for more details)

Table 1. Characteristics of the satellite data; ΔT, λ and $B_\perp$ are the temporal baseline, the wavelength of the sensor and the perpendicular spatial baseline between the master and slave images, respectively. The satellite frames are shown in Figure 1

Processing	Sensor	ΔT	λ	Track	Date (master)	$B_\perp$	Orbit
		d	cm			m	
InSAR	ERS 1/2	1	5.6	320	21 May 1996	37	Descending
				430	28 May 1996	62	Ascending
Speckle tracking	ALOS-PALSAR	46	23	661	1 August 2010	520	Ascending
				661	16 September 2010	437	Ascending
				661	1 November 2010	453	Ascending
				665	8 October 2010	588	Ascending

The yearly GNSS-velocities were acquired over several consecutive field campaigns, either December 2012-December 2013 or December 2013-December 2014, with a time span ranging between 362 and 368 days. Some of the GNSS velocity points served to calibrate the satellite-based flow fields and the others were used as control points.
Berger et al (2016) also compare the satellite-based flow field with 74 completely independent ground-truth measurements collected in 1965–67 (Derwael, 2014) and infer that "*The deviations are not larger than the uncertainty of our high-resolution flow field and we conclude that the RBIS has not undergone prominent changes in average ice flow over the last five decades*. "

To clarify, we have rephrased the sentence as "As shown in Berger et al (2016), comparison with on-site measurements collected in 1965-1967 and 2012-2014 yields no evidence of prominent changes in the ice velocities over the last decades, which supports the combination of data from different dates."

Line 25: "This dataset" – ambiguous agreed. We changed to "this velocity mosaic" (specifying before that the velocities have been mosaicked)
Line 27: Replace "cutting edges" with "seams" done
"Offsets between the two datasets are over 60 ma-1 in places." You are blending seams with feathering, but you are not actually correcting the offsets in velocity magnitude. The velocity mismatch at the seams varies from one place to another and can reach up to 60 m/a. As a result, it is impossible to remove the seams with a constant offset.
This will lead to smooth gradients for the divergence, but will likely lead to incorrect horizontal path determination for your Dh/Dt. That 60 ma-1 is a significant portion of the ~50-300 ma-1 velocities over the ice shelf. Your Lag Dh/Dt obs could be "off" by 6 pixels at your DEM resolution. The velocities are exclusively used to compute the divergence term. Also note, that the 60 m/a is a maximum deviation, the mean and standard deviation are much smaller . The DEMs are shifted with a normalised 2D cross-correlation. Shifting the DEMs with the velocities was less reliable because, as we explain in section 4.1, the velocity direction is not sufficiently constrained.

Line 30: "The SMB is based on…" is awkward start. You are using RACMO, not basing your SMB on RACMO. Good point, we changed to "We use the surface mass balance from a high-resolution (5.5 km posting) simulation of the Regional Atmospheric Climate MOdel (RACMO)..."
Line 32: Need a reference for these processes that RACMO is reproducing. We now refer to Lenaerts et al (2014)
Also, RACMO doesn't predict anything. 'predict' has been changed to "simulates"
Add reference to Figure 2b when discussing SMB spatial distribution. done

Page 6
Section 2.4: This section should be split into 1) DEM processing and correction and 2) Hydrostatic thickness calculation. We have divided this section in 2 subsections : surface elevations and

hydrostatic equilibrium.
Switching between “were” and “are” – should all be past tense To be consistent, we put everything in present tense
Add reference to TanDEM-X mission. Krieger et al (2007) added
Add reference for SARscape software? There is no peer-reviewed reference for the software that we are aware of but we have added a ® to indicate that this is a commercial software.
How did you co-register the DEMs? How do we know there aren’t horizontal and vertical offsets between your input DEM data that will lead to artificial elevation change (and LBMB) signals? As explained in subSection “Hydrostatic thickness”, we use a 2D cross-correlation to co-register DEM. The 2013 DEMs are tied with a simple offset to a CryoSat-2 DEM (Helm et al, 2014) and the 2014 DEMs are adjusted to the 2013 DEMs by fitting a plane, to correct for linear trends visible in the 2013-2014 difference fields. To do so, we have to assume that the absolute change in surface elevation between the two years is small.
Looks like a seam artifact is present in Figure 1 between labels 3 and B. LBMB values are positive (~3-5 m/yr) and then immediately adjacent, close to 0. Yes indeed, the LBMB data change rapidly over short distances because the value from 2 different frames (processed independently) are overlain. Frames boundaries are now visible in Fig S1 (Supplementary).
Line 12: Don’t start sentence with acronym agreed. Changed to “Digital elevation models” where it first appears then to “elevations”
Line 11: Based on my experience with Greenland data, I am skeptical of this 1 m vertical accuracy for TDM. This needs stronger justification. See reply G1.7
Line 18: What are dimensions of your Gaussian filter – 7 sigma is large, implying a large kernel, which will significantly reduce the resolving power of the output DEM (definitely not 10-m) See reply G1.10.
Weren’t the DEMs and GNSS data collected during different time periods? Are you assuming that no change occurred between the two collections? Yes we have to assume little change in the 6-10 -month period.
What is the “mean and standard deviation” of the differences? We subtracted the TanDEM-X elevations from the GNSS values and calculated the mean and standard deviation of subtraction.
The GNSS data are isolated to a small area, how do we know that this is representative of the larger ice shelf? The GNSS data used to determine the size of the filter are acquired over a square of ~20x25 km with abrupt topographic changes (Fig 1 – new). We use it to ensure that the filter does not smear out small scale details. Moreover we now also include a 100-km long, north-south oriented transect that covers 75 % of the along-flow extent of Roi Baudouin Ice Shelf to discuss the accuracy of the DEMs (reply G1.7)
Line 22: Wording is awkward, suggest something like “We calculate freeboard ice thickness assuming hydrostatic equilibrium…” Changed to “We invert the hydrostatic thickness from freeboard heights”
Line 25: Firn air content accounts for total air content of the firn, not variable firn density. To be clearer, we have rephrased the text : “The firn-air content Ha accounts for the lower firn and snow densities by subdividing the ice column....”
What are typical mean dynamic topography offsets for this location? In our area of interest, the mean dynamic topography ranges from -0.9 to 0.6 m (with an average of -0.1 m) . This is now specified in Table 1
Are you accounting for density errors in your uncertainty estimates? I’ve found that including a +/- 5 kg/m3 uncertainty in density can dominate the freeboard thickness error, much more than a few meters of firn air content error. This comment is a little unclear. Uncertainties in firn-air content do implicitly mean errors in the (depth-averaged) density. Do you refer to the assumed ice density (e.g. 900 vs. 910 vs. 917) ? For a thickness of about 300 m, changing the assumed density of ice by 5 kg/m^3 has the same effect as changing the firn-air content by about 1 m (both cause 6-7 meters thickness change in the hydrostatic ice thickness). The uncertainties due to density are discussed in section 4.

I've found that IMAU-FDM estimates over ice shelves in West Antarctica are biased high, in some places 5-10 m too high, compared to radar-derived firn air content using techniques from In our case, the firn-air content from IMAU-FDM deviates with 0.7+/-2.0 m (with a maximum deviation 3m) of from radar-derived firn air content in Drews et al (2016), who analysed 5 wide-angle surveys, including 1 data point in an ice-shelf channel where the results were verified with ice-core data.

Review was interrupted for several weeks at this point. Picking up again. I apologize for discontinuity in comments.

Line 28: What is approximate mean dynamic topography correction for this location? See reply p6, L25

Page 7
Line 5: I think you mean "these approaches are not well-suited…" True but the whole sentence has now been rephrased to be more specific. "However, smoothing prior to taking the derivative can lead to smearing out of the derivative in areas where the derived quantity changes abruptly (or discontinuously)."
Line 9: What is meant by "wiggliness" of the derivative? Need a little more explanation about what you are solving for and how the process works. This is emphasized as a novel method, so it should be documented clearly. Agreed. The wiggliness refers to the second derivative which becomes very large if the data are noisy (this because the finite difference schemes pick up the local slope of the noise as opposed to the larger scale signal). We have rephrased section 2.5 (including a comparison with smoothing the data to different degrees). See also reply G1.1.

So, you are computing horizontal and vertical gradients separately, then combining in a large inversion? We use the regularized derivative separately for x and y and then combined them
How does the velocity map resolution impact alpha? The map resolution indirectly influences alpha in the sense that lower resolved velocities (i.e. spatially averaged and less noisy) require less regularization when taking the derivative and vice versa.
When I look at Figure 2D, I still see plenty of noise in the velocity divergence map. We have justified our choice of alpha (i.e. the regularization). As prescribed by (Chatrand, 2011) we use the discrepancy principle to choose our alpha, i.e. we rely on the estimated noise in the velocity field.
Line 18: replace "such as" with "including" done

OK, so you de-tided the GPS surface elevation data. Yes. Did you also detide the TDX DEMs? Yes, indirectly by calibrating the TanDEM-X DEM (with the grounded parts masked out) to a de-tided DEM
What depths were the reflectors used to determine strain thinning? Did you have to account for firn compaction? The strain thinning is based the bottom of the ice shelf and upper reflectors located 60 to 90 meters below the surface. Therefore, we don't need to account for firn compaction.

Page 8:
Lines 1-2. I don't understand this. You are saying the strain correction is small compared to the basal melt rate, with both provided in units of m/yr. This makes sense. The 10-day interval should be irrelevant here – why is it mentioned? Thanks for pointing this out, the strain rate should have units per year (not meters per year) and we have removed the part about the 10-day interval. Also correcting for strain thinning is standard in pRES processing (also when it is small).

This result about strain correction suggests that the velocity divergence term (and the regularization) is not necessarily important for the larger shelf LBMB calculation. The Correct. We

have mentioned that in the old version on p13 L30-31 (old) " Fortunately, for the Roi Baudouin Ice Shelf this effect is mitigated by the low ice-flow divergence,[...] This may be different for other ice shelves." The pRES data are in an area with low divergence.
Line 6: "seaward" done
In Figure 1, what is the band of large positive (blue) values along the grounding line to the right of Label "1"? Artifacts or real refreezing signal? My guess is that the Depoorter grounding line is in the wrong place, the ice at this location is grounded, and this area should be masked.
We don't know what is causing this band. A mislocation of the grounding line seems unlikely, as we have checked numerous grounding lines in this area, many of which coincide with ground-based measurements and show little temporal variation (Drews et al., 2017). Potentially the band is linked to unaccounted surface processes such as melt water formation which can be abundant in this area (Lenaerts et al., 2017).

Line 8: "stoss" is a relative term – could be leeward for ocean circulation, different direction for wind, different direction for ice flow – suggest changing to absolute direction ("south") agreed. Changed to "southern"
Line 11: Where are these overlapping areas? Are you sure that the LBMB is not changing over the period for which you are performing the analysis (could some of your observed std be due to real changes in melt rates?) I think you are saying that formal error estimates are larger than the magnitude of the measured signal.
The overlapping areas of the LBMB coincide with the areas where 2013 and 2014 TanDEM-X frames overlap with other frames of the same year but different dates. This is now shown in Fig S1 (supplementary). We have no handle on the temporal evolution of the LBMB, but all the TanDEm-X DEMs have been acquired during Austral winter. It is correct that our error estimates are larger than the signal. Therefore, we use these difference fields in LBMB as a lower boundary for our error estimate.

The last sentence on Page 8 and first sentence on Page 9 have no real context. I think you are making an argument that dh/dt from sparse or low-res measurements is problematic. But you have high-res DEMs, so you don't need external datasets for high-res Eulerian elevation change. Agreed, this section has now been rephrased and the part about "the need for external datasets" removed.

Page 9
Line 7: Is this order of magnitude difference present everywhere? Seems like DH/Dt values are close to 0 in the middle of the shelf, so the vdiv and smb terms become much more important. Good point. Overall the DH/DT term is the most important one. In some areas (where this term is close to zero) other terms are equally important but in those areas the LBMB signal is typically very small and close to the detection limit.
Line 11: Is this convergence within channels present across the full channel width, or just on the sides, or do you lack the resolution to determine this? This convergence pattern appears clearly in modelling studies (most prominently in the flanks), but is hard to pick up in observed surface velocity fields.

I don't see negative Dh/Dt across all channels in Figure 2f. In fact, I see positive Dh/Dt in several places (e.g., just northwest of the right-most arrow in figure 2d)." So, the convergence is causing thickening of the ice shelf at this location? More likely is that you are picking up surface elevation change due to snow redistribution.
It is correct that not all ice-shelf channels show the same pattern. However, some do and we link those to the modelling results of Drews et al., (2015). It is entirely possible that we also pick up some local changes of the SMB (as stated in Section 4.3 - old). We included that point in the revised manuscript.

Page 10
Line 3: At the channel center, LBMB values are positive, potentially even +2-3 m/yr. This is not close to zero. What is going on here? Is that refreezing (unlikely) or is this an artifact? Need to address this if you are going to interpret the signals on the sides with confidence.
The absolute LBMB values are inflicted with an error that is larger than the signal. The key observations here is therefore that the absolute magnitude of the LBMB is 3 times higher in the flanks compared to the channel's centre (-5 m/a vs 1.5 m). Our emphasise is much more on the spatial variability than on the absolute values. Because enhanced melting at the channel's flanks has been suggested for wider ice-shelf channels (Millgate et al, 2013), we find this observation meaningful even if uncertainties remain.
Line 4: not km2 here, just km done
Line 4: elliptical, not ellipsoidal replaced there and elsewhere in the text
Line 5: You don't necessarily know that the lake is connected. It's location is adjacent to the channel, but careful about wording that could be misinterpreted here. Changed to "elliptical surface depression [...] located on the upstream end of an ice-shelf channel"
Line 6-7: This interpretation about tributaries needs more support if it is going to be included. We have now replace the term tributaries with "fingers", which is used to describe the location and shape of the features feeding into the elliptical surface depression. We don't do any interpretation beyond that.

I haven't seen the Lenaerts et al (2017) paper, but I'm puzzled by this interpretation. Are you suggesting that the lake is liquid water, 30 m below the surface of the ice shelf? Why have these not refrozen? As explained in reply G1.3, we have made it much clearer here that there are multiple options that could explain this feature but that if it was a lake it has probably refrozen.

Line 12: "blocks the penetration" suggest "attenuates" We mean blocking in the sense of total reflection and negligible transmission.
This interpretation is inconsistent with the radar data shown in Figure 6. There are many reflections beneath the "lake" feature. This to me suggests there is no way that this is liquid water. There may be an interface that is attenuating the radar signal, but definitely not salty water, which seems like the only way to prevent refreezing. As stated above (p10 L6-7), and in the initial manuscript, we also consider that the interface is a refrozen (formerly liquid) lake. The revised version is correspondingly adapted to make this more clear. There are no radar signals originating from beneath the prominent interface (we have checked this with phase sensitive radar). The signals that occur at larger depths in Fig 8a(new) originate from off angle reflections from the lateral walls.

Line 15: I disagree – this interpretation is important. I would not call it an englacial lake if you have no direct evidence for this interpretation. Stick with "elliptical surface depression" and be consistent throughout. Agreed. See reply G1.3
I am not entirely convinced that the apparent LBMB over this feature is not due to variable snow accumulation and redistribution over the periods when you have elevation measurements. True, changes in SMB could, in theory, impact our LBMB. However, previous studies suggest higher accumulation in surface depressions (Langley et al, 2014) and at the bottom of slope (Frezzotti et al, 2007). Increased SMB at this location cannot explain surface lowering as it would decrease the inferred melt rates. As a result, unaccounted SMB variability would make this signal even more prominent. We don't see a mechanism why snow would be redistributed (by wind) out of the surface depression.
I disagree with the interpretation that the pRES and DEM-derived LBMB values agree "well" or show a "near-perfect" fit. Figure 6b shows major disagreement (+/-2-6 m/yr) between the two in places. These offsets are large and significant compared to the magnitude of the LBMB signal. See reply G1.4

This paragraph is very long, and should be broken up Done

Line 19: I don't think "low" is the right term here, try "large negative" done
In Fig 6c, I don't understand why the surface is getting lower over the depression, but getting higher between 0.5-2.0 km. Actually, the surface is also getting lower between 0.5-2 km (the black line is the oldest profile). So, if I understand correctly, the P-P' profile was extracted in a fixed Eulerian 2016 location? So some/all of the observed elevation change for this fixed profile could be due to advection? Why was not extract the profile in a Lagrangian sense, moving with the feature? The profile shown on this figure is already in a Lagrangian framework, i.e. the TanDEM-X DEMs have been moved forward to match the acquisition geometry of the 2016 GNSS profile. As a result, we don't think that the observed elevation changes are due to advection.

Are you convinced that you are not seeing penetration of the radar into snow and ice in the TandDEM-X DEMs? Other studies have shown this can be several meters, potentially up to 10 meters in cold, dry snow. This could impact the comparisons with GNSS surface elevations. Yes , see reply G1.8

It looks like the large negative values in LBMB along the channels is mostly coming from the velocity divergence term. Are you confident that these negative values on channel sides are not artifacts velocity resolution and regularization approach are a [word missing, we do not understand the end of the sentence] The three figures below present the different term influencing the LBMB in Eq (1) but unlike Fig. 2, in the paper, they are presented with the same colorscale. Looking at these maps, gives us confidence that the negative LBMB values on channel's sides are driven by the DH/Dt more than by the regularization.

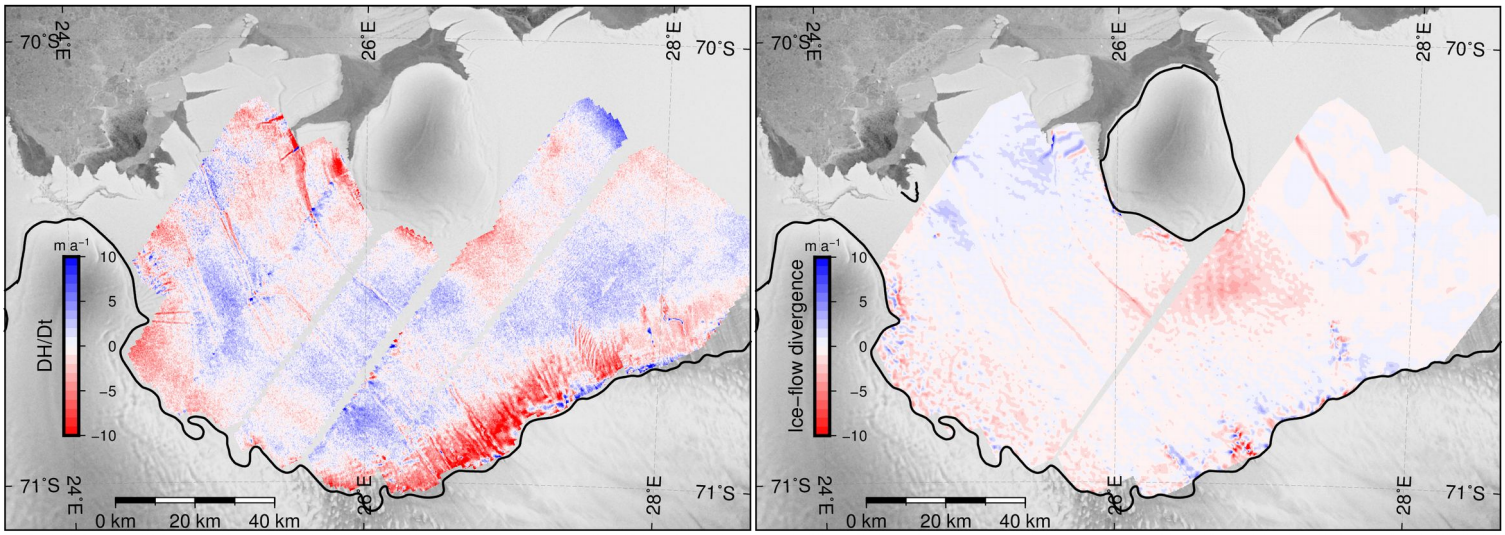

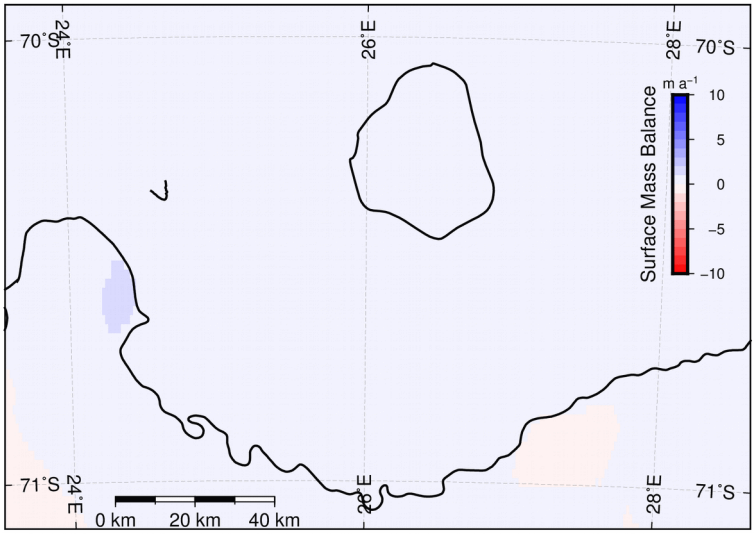

Line 25: Again, no evidence for connection. Inactive in what sense? You don't see an elevation change signal, so it is not actively experiencing melting or refreezing. Changed to "the ice-shelf channel located farther downstream does not show strong surface elevation change suggesting that it is not actively melting or refreezing."

Line 28: How does an englacial lake creep through an ice column? Is there a reference for this, or is this your interpretation? Still don't understand how this could remain unfrozen. See reply G1.3 However if the water were to remain liquid, density difference between liquid water and frozen ice could result in a net-downward force causing creeping.

Lines29-30: Not sure what this sentence contributes. This sentence is there to show that even though we cannot be sure of the processes happening at the depression, our technique is able to detect small-scale processes from space. We have rephrased the sentence : " this example highlights that much of the small-scale variability seen in the resulting LBMB field can be used to investigate sub-kilometre-scale ice-shelf processes that do not necessarily occur at the ice-shelf base " I'm still thinking that much of the observed elevation change within the depression could be due to local surface accumulation and wind redistribution. See reply p10, L15

Page 13:

Line 5: This is also highly dependent on the density ratio of ice and ocean water, not just the firn air correction. True. We have rephrased the sentence to mention this :

"The Lagrangian thickness change depends (i) on factors controlling the hydrostatic ice thickness, i.e. the surface elevation (above sea level), the seawater and icedensities, the depth of the firnpack and temporal variations thereof; and (ii) on the Lagrangian matching of the DEMs following the ice flow."

Line 11: Do you mean overlapping DEMs? Yes and we have replaced neighbouring with overlapping

Line 13: "cutting edges" – I think you mean "differences exceeding 13 m/yr across seams" yes, changed

Line 15: OK, but isn't there a 2-year time difference between the DEM timestamps and the GNSS measurements? Is this an appropriate comparison? You are right, we are now comparing the 2013 and 2014 DEMs with a GNSS data from 2012 and 2014, respectively. (see reply G1.7). With these smaller time periods, we believe the comparison is now more appropriate.

These offsets in the firn air content are significant. What percentage of the total ice thickness is this? In some cases ~5-10%? These offsets represents between 2.5 % and 3% of the total ice thickness

Line 29: Also, can have surface and basal crevasses, filled with ice/water/air that will affect the air

content. Maybe less relevant at these locations. Yes we believe that this is less relevant here.
Line 34: "To get our LBMB in Lagrangian geometry" – I think you mean "to determine the relative offsets between surface features in the two DEMs, needed to compute Lagrangian Dh/Dt…" We have rephrased the sentence : " Computing the Lagrangian thickness change, requires matching the DEMs to account for ice advection. We use a normalised cross-correlation to match 5×5 km patches from 2013 to the 2014 geometry (Sect. 2.5)."
These are length and width in km, Not km^2. Agreed, changed
Line 35: Correlating DEMs is not always better, esp for smooth, featureless surfaces or sparse altimetry data. Agreed we rephrased that part.

Careful about comparing magnitude of "SMB" here, which is m w.e. – you are using the expected elevation change output by a firn model driven by SMB, right? Not the same thing. No, as stated in on p3, L7 (new) "Mb, Ms and H are given in ice-equivalent units." so it is ok to compare magnitudes here.

Page 14
Line 3: Bimodal is not the right word. I think you mean a positive/negative signal due to misalignment. Agreed. Changed to "positive/negative"
Line 4: So which did you use again for the paper? I thought you were using existing flow fields, not your cross-correlated flow fields? Make sure this is clear wherever it is discussed in the text.
We are using the flowfield derived in Berger et al (2016), which compares well with GNSS measurement. To make it clearer, we have moved the reference to Berger et al (2016) a bit before.
The differences between the two approaches in Fig 7 are not as drastic as one would expect. Why did you choose 5.125 km window? This is a 41 pixel window for 125 m velocity maps! I would chose something far smaller, like a 3x3 px, 5x5 or even 9x9 px. My guess is that such a filter would remove noise but preserve the same channel-scale divergence as the regularization. It's not really a fair comparison to say that your method is better than smoothing when you only tested one very large smoothing window. I'd also like to see the original data, so we can assess the improvement offered by the different approaches.
As explained in reply G1.1, we have updated Figure 3 (new). You were write to guess that smaller average filters also remove the noise. However, all of them seem to under-estimate the amplitude of the convergence inside the channel. The regularised divergence, on the other hand, seems a good trade-off that accounts for the convergence of the channel but at the same time smooths the signal.

Line 15: OK, earlier you made the argument that the velocity divergence term was small, so the error in firn air and hydrostatic thickness was negligible. Now you are making the argument that the velocity divergence term is significant. Agreed. We are now clearer that it might be important for ice shelves with strong dynamic thinning.

What is the error from a 10 m error in firn air correction for the entire shelf? Might be an informative map, which could be used to produce a map of uncertainty in LBMB. I think Moholdt had some nice figures like this in his paper.
Thanks for your suggestion. Instead we have referenced the error analysis of Moholdt et al. (2014) and discussed error sources specific to the Roi Baudouin Ice Shelf in Section 4.
[P14]
Line 23-24: You're not really applying an atmospheric model, you are using output elevation change products from a firn densification model (FDM) driven by regional climate model (RACMO) outputs. We changed "applied" with "used"

Line 24: Could also be overestimation, which would have negative bias. As stated above (reply p10, L29-30), we don't see a mechanism how snow can preferentially be redistributed out of the

channels and we are not aware of any observational evidence supporting this idea. On the other hand, there is evidence for a locally increased SMB inside ice-shelf channels (Drews et al. 2015, Langley et al, 2014). Therefore, we only mention the positive bias here.

It's important to separate SMB from elevation change due to SMB. SMB is in m w.e., while the actual elevation change will depend on density of snow and firn. Fresh snow will have a lower density, and potentially a greater impact on elevation change. Agreed. As we only use a time-averaged SMB, we cannot account for that effect but it is now mentioned in the text.
Line 28: What is the approximate length scale of the tidal flexure here? The length of the tidal flexure zone is spatially variable and can extent more than 6 kilometers (Drews et al., 2017).
Line 29-30: Suggest that you state the datasets used – ICESat-1 was used to infer ice thickness. Ice thickness in Rignot et al (2013) is from BEDMAP2 (Fretwell et al, 2013) and thickness change from ICESat-1**.** We know specify the origin of thickness changes "(i.e. ∂H/∂t based on ICESat-1)"

Page 15
While slope may very well be an important factor here, the shelf draft is significantly deeper near the grounding line, where we would expect a suppressed freezing point and enhanced melting. Like some combination of these two factors. Indeed we now mention the depth.
Line 3: "observed variability" in what? LBMB? LBMB added
Line 4: Why only surface lowering? Really it's more general – surface elevation that is not representative of hydrostatic ice thickness. Changed to "surface elevation change"
Line 8: "This indicates" – the datasets don't' make the region active changed
Line 10-11: I still don't understand how a liquid body can "creep" through the ice column unless it has high salinity. See reply G1.3.
Line 12: "appears passive" – not sure what you mean by this. I think you mean that the apparent basal melt rates are small. We added "(i.e. does not show significant melting nor refreezing)"
Line 15: "connected to the grounding line" – the channels appear to originate near the grounding line, but this does not necessarily imply a direct connection. Some of the channels can also be inherited from bed topography at the grounding line, which leads to feedbacks in basal melt magnitude/distribution. This claim is substantiated by the findings of Drews et al (2017), Le Brocq et al (2013) and Sergienko (2013). Moreover, Drews et al (2017) use ground data to show the connection between 3 ice-shelf channels and the grounding line of the Roi Baudouin Ice Shelf.
Line 17: Be sure to specify that you are talking about subglacial meltwater originating upstream beneath grounded ice. "subglacial conduits injecting subglacial-melt water into the ice-shelf cavity", already implies that the water comes from beneath the grounded ice.

Page 16:
Line 1: Cite Shean (2016) See response p4,L7
.[Dutrieux et al., 2013] noted that melting appeared to be focused in channels near the grounding line and on keels near the outer shelf. The full-shelf thickness gradient at PIG is substantial, 1- 1.5 km near the grounding line, and 300-500 m near the calving front. I believe there is also some component of Coriolis that can lead to asymmetric melt within the channels. You are right, but in our case we do not see a significant left-right asymmetry in the LBMB rates.
Line 11: "sub-kilometer" done
Line 14-15: So, over what length scales are pRES point measurements representative? As a rule of thumb we would say that the pRES measurement represents the surrounding area where the ice thickness is approximately constant. The exact value then depends on the specific ice shelf.
Line 16: "uncertain in their magnitude" – so you are suggesting that satellite LBMB on its own is not useful? I disagree. I think it's also a matter of LBMB signal magnitude. At PIG, melt rates exceed 200 m/yr in places, so 5-10 m/yr error is negligible. As here we tie the DEMs to each others (during the plane fitting), our technique is better at determining the spatial variability of the LBMB that its absolute value.

Line 18: “we derived” done
Line 19: This makes it sound like you ran an atmospheric mode. Replace “atmospheric modelling” with “elevation change output from a dynamic firn model driven by regional climate model output” changed to “atmospheric modelling outputs”
Line 20: deepest and steepest. done
Line 22: Really, you are not observing large basal melt rates below ice-shelf channels, you are observing high melt rates beneath surface depressions that form over basal channels. We define an ice-shelf channel as a curvilinear tract where ice in incised at the base and forms a depression at the surface of the ice shelf. Moreover we clearly state in the text that “It should also be clear that our approach is only able to detect basal changes reflected in the surface elevations, because ice thickness is derived from hydrostatic equilibrium.”
Line 25: I’m still not clear on the matching procedure – did you combine your independent velocities and your velocity maps derived from DEM correlation? Restate the actual procedure that offers improved quality here. See reply G1.6 and section 2.5(new) where we better explain the matching. We added “ -- a normalised cross-correlation coefficients --”
Line 27: “…small-scale flow anomalies (e.g., channel margins)” changed to “...abrupt changes in flow velocities, which are sometimes observed across ice-shelf channels.”

Tables:
Table 1: Mixing km and degrees in the “gridding” column. We know it is unfortunate but that's how the datasets are provided meaning that for some datasets the gridding is spatially variable.

Figures:
I might reorder these figures to build to the LBMB map. You could show the components (Fig 2) and the Eulerian map (Fig 3) first, then LBMB map (Fig 1). See reply G1.13

Figure 1: Delete “in slight transparency” Done

Figure 2: Which surface velocities are you showing – the InSAR-derived products, or your velocities from cross-correlation of TDM? We show the InSAR derived velocities (see reply p4, L10). To make sure the readers are clear with that, we refer to Table 1.
In panel d, what is the ~30 km long linear feature to the east of DIR? Is this an artifact? There doesn’t appear to be any channel in the ice thickness map. I’m guessing this is where you used the Rignot et al velocities. Should add something about this in caption. Yes this is an artifact in the velocities from Rignot et al (2011). The caption has been updated with “(Note: the red lineation 30km east of Derwael ice rise is caused by a seam in Rignot et al (2011)'s flow field)” and we have now delineated the flow field from Berger et (2016) in Fig 2c.

Figure 3: What time period is shown here (ie what is dt)? Is this eulerian dh/dt from your 2013 to 2014 DEMs? I don’t think you mean steady state here – you are showing observations, right? The shelf could still be thinning/thickening in Eulerian frame. We meant steady state but we have updated the figure: we now show panels : the Eulerian thickness change, the flux divergence and the Eulerian BMB. (see reply G2.2 to reviewer 2)

Figure 5: Mention arrows in caption. Although I don’t think these features are necessarily worth noting (there is also a similar depression on the other side of the channel). We have removed the arrows. Are the 5-10 m/yr freeze-on signals (near P) in panel B real? We are confident about the pRES results, less so about the absolute values of the LBMB.

Figure 6: Why is there a large offset between your GNSS surface (~60 m on the y-axis) and the reflection from the surface in the GPR profile (~10 m on the y-axis)? Shouldn’t these be in the same place? During the radar processing we muted parts of the direct wave, this is what causes the

apparent offset between the GNSS surface elevation and first signal in the radar data.
When the GPR data were processed, did you use 10 m or 1 m of firn to convert two-way traveltime to depth? For the profiles near the grounding zone we used 1 m. The density correction in radar-traveltime, however, only results in a few meters difference regardless of the estimated firn-air content.
What dates (month, day) from 2013 and 2014 are you showing here? Don't you have many DEMs from each year over this location? The legend of panel (c) has been updated to specify the dates of the profiles.

Figure 7: It would be useful to see another column here with the divergence and LBMB from the original velocity data for comparison, so we can see the improvement offered by your regularization. Very good idea. The figure is now very different from the previous manuscript but we now show the original data. see reply G1.1
I don't understand why there is still so much noise in panel d. This suggests that the elevation change measurements from the TanDEM-X products are the source of most of the noise in the final LBMB maps. Yes it is stated in Section 4.1 that primary error source is the DH/Dt (thus the elevations) Eyeballing this figure, if I were to draw a window around the lower quadrant and compute a standard deviation of these values, it would probably be something like 1-1.5 m/yr. Is this consistent with your stated vertical accuracy of <1 m?
This part of the ice shelve is not appropriate to draw a window, as elevations change too much, due to (less visible channels). If we take a 7 by 10 km box, in a flat area of the ice shelf (this is not the case of the lower quadrant) and we difference the 2013 and 2014 DEMs (in an Eulerian framework, as this area is featureless). The mean difference and its standard deviation are 0.65+/-0.15, which is consistent with our stated accuracy.

Response to reviewer 2 (Geir Moholdt)

Current mass losses from the Antarctic ice sheet are dominated by ice-shelf basal melting, but yet we know relatively little about the variability of basal melting and refreezing at the scale of individual ice shelves. This paper uses various high-resolution datasets from remote sensing to derive a detailed map of basal mass balance for the Roi Baudouin ice shelf in East Antarctica. The applied data sets and methods have several novel aspects, and the results are interesting in both a glaciological and oceanographic context.

The paper is well written and easy to follow. The methodology is well described, the figures are clearly presented, and the discussion is straight to the point. I have a few general issues/questions and some smaller comments/edits as given below.

G2.1 Lagrangian vs. Eulerian: I think the authors exaggerate about the "necessity of the Lagrangian approach" (P8, L15), at least if they mean it to be generally applicable. I agree that it is by far the best approach with the data sets they have at hand; i.e. two high-resolution DEMs that can probably be more accurately co-registered to each other (Lagrangian) than to an absolute reference system (Eulerian). But if consistent elevation and velocity data were available, there would be nothing in the way of getting reasonable Eulerian results. Agreed, we have changed the text accordingly and show the Euler results.

G2.2: In fact, the authors fail to show that the Eulrian approach does not work in their case because they do not try to calculate Eulerian thickness changes. As long as the DEMs can be consistently georeferenced, it should not be much extra work to calculate and account for that to obtain real Eulerian BMB in Fig. 3. I do not doubt Lagrangian is better, but it would be nice to see it demonstrated as a comparison to the patterns in Fig. 1. Agreed.
Following your advice, we have modified Fig. 3 (Fig. 5 new) : we have removed the steady-state BMB and replaced it by 3 panels. One with the Eulerian dH/dt, a second one with flux divergence and the last one with Eulerian BMB. Arrows in the figure locate places where the Eulerian approach fails. The text has been adapted.

G2.3 Ice shelf mass balance: The authors do not provide overall estimates of any mass balance components. That could be because the data sets do not cover the entire ice shelf or because they think that inherent biases are too large to do it confidently. However, I think that even some rough area-averaged estimates would be useful to include, or at the very least you should explain why this was not done and which challenges remain to be able to do it. Would flux gate methods be more reliable for that purpose? Potential biases between the 2013 and 2014 DEMs should be possible to correct quite well with CryoSat-2, whereas changes in firn air content and ocean properties are probably more difficult to assess.
Indeed, we did not provide any overall estimate due to the incomplete coverage of RBIS and the very large uncertainties, compared to the signal magnitude. We now specify that our spatially averaged LBMB rates correspond to a net basal loss of -6.7 Gt/a. Also, as we tie the DEM to each other (during the plane fitting), our technique is better at determining the spatial variability of the LBMB that its absolute value.

Specific comments and questions in chronological order:
P1, L9: Is this range an estimate of actual min/max BMB or does it also contain impact from measurement noise? I guess that some erroneous values would be even larger. Correct, the actual min/max BMB ranges from -77.9 to 233.3, which is clearly unreliable. Instead, -14.7 to 8.6 correspond to the 0.1st and 99.9th percentiles. It is now clearly stated in the text.

P1, L11: Can be interpreted as if the radar profiling is an error source. Perhaps more clear to say something like: "...although independent radar profiling show..." Thanks for pointing that out. It has now been rephrased as “although independent radar profiling indicates unresolved spatial variations in firn density”

P2, L1: has emerged done

P2, L17: ice-sheet promontory. We are using the term defined in the literature by Favier et al (2016): “Ice promontories are ice rises that are connected to the mainland through a grounded saddle.”

P2, L24: specify "several uncertain quantities" rather than just "large numbers"? Agreed. Changed

Fig. 1: I got a little bit confused about the letter labelling (a, b, c) and the panel labelling (a, b, etc.) in the later figures that they are connected with. I suggest to rather label the frames with the figure numbers they refer to (4, 5, 7) and then the three regions of interest with letters, like A, B, C.
Very good idea. The figure and the references in the text have been adapted

P4, L1: Euelrian also requires two thickness fields in time to calculate dH/dt. In that sense, I do not see any difference with the Lagrangian approach. It is only the reference frame that is different (fixed or moving). See the general comment about this issue. Agreed. See replies G2.2 and p4, L1 of reviewer 1.

P4, L28: Any suitable reference to this technique? Yes we have added the reference “(e.g. Joughin, 2002; Neckel et al, 2012)”

P4, L24: Can the coverage of these three velocity datasets be indicated in Fig. 2c?
That would be helpful for interpreting noise and smoothness in the divergence field in 2d. We have now updated Fig 2c to indicate the coverage of the different datasets, though some seams directly come from the velocities in Rignot et al (2011a) such as the red band on the east of Derwael ice rise in Fig 2d. (this is specified in the caption).

P6, L13: Depoorter et al. (2013) is a composite grounding line from several other published ones. What is the real source in this case? Thanks for reminding us of that. The text has now been changed to “Grounded areas are masked out using the composite grounding line from Depoorter et al (2013), based on differential InSAR with Radarsat and PALSAR (Rignot et al 2011b) at RBIS”

P6, L26: Do you use a steady-state firn air content or a time variable one? The SMB and firn air content we use are averaged over the periods 1979-2015. This is now specified in Sections 2.3. and 2.4 (hydrostatic equilibrium) In any case, changes in firn air content (mainly due to accumulation anomalies) are a major uncertainty for the derived thickness changes because errors get incorrectly magnified by a factor 10 in the freeboard-to-thickness conversion. This should be mentioned. We have now added a few words about this in section 4.1.: “Because of unaccounted variations in firn density, and uncertainties in referencing the freeboard height, our ice thickness field has a lower bound error of at least ±25 m (Drews, 2015). In some areas the error can be considerably larger. However, the corresponding impact on the inferred LBMB rates is mitigated by the low ice-flow divergence rendering the magnitude of ice thickness less important (Eq. (1c)).

P4, 13: This level of detail does not really fit here in a general description of the sections. I would rather describe the DEM differencing at the end of section 2.4 with a little bit more detail than here. The method and 5x5 km processing is not completely clear to me. Agreed. We have created a new section “Lagrangian thickness change” where we explain the matching procedure in greater details

(see reply G1.6 about the reshuffling of the method section)

P6, L28: What about corrections for ocean tides and the inverse barometer effect? The 2013 TanDEM-X DEMs are tied (with a simple offset) to the cryosat 2 DEM (Helm et al, 2014), which is itself corrected for tides (using CATS2008a) and inverse barometric effects. We assume that both effects uniformly lift up the ice shelf and that therefore the calibration removes them.
As for the 2014 DEMs, they are adjusted to the 2013 DEMs during the de-trending step, which means that they are also indirectly corrected for tides and inverse barometric effect. (This also means, that our method assumes that no significant large-scale thinning/thickening occurred between 2013 and 2014). We now mention this in section 2.4 and 4.1.

P7, L11: Fig. 7 is a very nice illustration of this improvement, but is not shown until page 15. I think it should be moved forward here (Fig. 3?) since it helps to understand the purpose of the methodology. Thanks for the suggestion, it has been moved to section "spatial derivatives with noisy input data"

P7, L27: Should be mentioned earlier together with the DEM methodology. Thanks for the suggestion. However, we would prefer to keep it as it as because the use of GNSS elevation to extend the time series is really minimal to discuss the elliptical surface depression.

Fig. 3: I do not really see the relevance of this figure since we know that Eulerian elevation changes have a very variable pattern due to advocating topography. Assuming steady-state dH/dt is not a valid approach for determining spatial patterns of BMB, only area-averaged BMB. As mentioned earlier, I would rather like to see 2-3 panels with dH/dt from DEM differencing, maybe also u*div(H), and Eulerian BMB accounting for both of those contributions. See reply G2.2

P8, L8-9: Label 2 and 3 are switched. Done

P9, L1: Why does it need to be "prescribed from external datasets"? Why not use your own DEMs? Agreed. We now explain that spurious signal arises when Eulerian thickness changes is taken external datasets. At the same time we now show the Eulerian BMB calculated with our DEMs.

P9, L3: The term steady-state is confusing here. I would rather highlight that it violates the ability to derive spatial patterns of basal melt. We have rephrased that part : "hence introducing artifacts in the basal mass balance pattern."

P10, L2: Nice to be able to see this! Thank you

P10, L20: I would say opposite. Surface lowering is caused by negative LBMB. Actually, we can't be sure that it is due to basal melting. So we've rephrased the sentence :"The large negative LBMB rates in the elliptical depression reflect persistent surface lowering of 0.5 to 1.4 m/a ; ice-flow divergence is negligible at that location."

P13, L34: I agree, it is better to use the same data directly than external sources. Thanks

P14, L5: This is a good novel approach. Well done. Thanks

P14, L27: I agree, but what about the channels? The effect of incomplete hydrostatic equilibrium across the channels is not discussed much (e.g. in relation to Fig. 4). Very good point. We now mention "The smaller-scale variations in LBMB are more difficult to interpret, because these are overlain by unaccounted variations in firn density, SMB, and ice that is not in hydrostatic equilibrium."

P14, L30: Is the gradient more important than the absolute thickness? The latter is not discussed, but is important for the pressure melting-point of the ice. We briefly discuss the pressure-melting point

P15, L17: Reference Drews et al. 2017, Nature Comm. Done

P16, L14: Good point! Thanks

Response to Rupert Gladstone's informal comments

Interesting work!

Fig 4, really interesting to see the detail here. Please add a label other than 60 so we don't have to count contours! Done, contour lines are now labelled every 5m

You might want to add a subplot here showing actual thickness if you have it, or maybe hydrostatic thickness if you don't as the basal expression of this feature is presumably much deeper than the surface expression. Unfortunately, we only have hydrostatic thickness available in this area and we don't think that adding a new panel with thickness would add much here because all the other datasets used for the hydrostatic inversion are too coarsely resolved to influence thickness changes over a few km. As a result, thickness changes in that area roughly correspond to elevation changes multiplied by 10.

Fig5, again additional contour label in a and b would be good. Please describe arrows in the caption. Arrows have been removed and we have added additional contour labels.

Fig 7, it is hard to see the channel location here. Would elevation contours help here? Or something to clarify the location of the channel, which gets a bit lost especially in c,d. In fig 7c I am guessing that the red region is on the channel side and the blue region is the middle of the channel, but some visual clarification of this would be useful. The maps are now overlain with contour lines.

Given that channels appear to melt preferentially at the side, why do they not just keep getting wider? Is this balanced by lateral convergence of the ice flow? You mention lateral convergence in the context of data processing, but perhaps this should also be mentioned in your discussion of melting in sub-shelf channels. Good point. It seems that melting at the sides does not persist over the entire length of the ice shelf, which would be one reason preventing the channels to wide. Lateral convergence may be another. The later is explicitly discussed in section 4.2
Could you view it as a competition between the ice dynamics trying to close these channels through lateral convergence and the ocean dynamics trying to open them through preferential melting at the side walls? Are there circumstances under which one would win over the other or are there feedbacks that prevent either from winning? Perhaps preferential side wall melting would steepen the side walls causing an increase in lateral convergence? You could see the lateral convergence as a response of the ice shelf to basal melting. Drews, (2015) explain : "basal melting reduces the ice thickness inside channels and causes vertical velocities at the ice-shelf bottom to be negative. This increases the vertical strain rates (Ezz) inside the channels, causing subsequent lateral convergence (Eyy) while longitudinal stretching (Exx) is only slightly affected". Without basal melting lateral

lateral convergence also ceases and at least for the cases we have looked at this effect is not strong enough to fully close ice-shelf channels.

Did you think of using statistical techniques to investigate the relationship between LBMB and potentially relevant parameters such as spatial gradient of the ice shelf lower surface, absolute depth of the lower surface, distance from grounding line? This would shed some light on the relevance of currently used basal melt parameterisations (which are mostly linear functions of depth) in marine ice sheet modelling. Perhaps this would be a separate study, but really someone should be doing this urgently, and you have a good data set for it here! I feel sure that one could empirically justify a melt parameterisation as a function of both slope and depth more easily than just depth. Thanks for the suggestion, we agree that this would be useful information but we think that this would be out of the scope of this study. We are nevertheless considering investigating the parametrization in a separate study.

Bibliography

Berger, Sophie, Lionel Favier, Reinhard Drews, Jean Jacques Derwael, and Frank Pattyn. 2016. "The Control of an Uncharted Pinning Point on the Flow of an Antarctic Ice Shelf." Journal of Glaciology 62 (231). Cambridge University Press: 37–45. doi:10.1017/jog.2016.7.

Derwael, J.-J. 2014. "Snow Accumulation Data: Princess Ragnhild Coast, Antarctica. Belgian - Netherlands Antarctic Expeditions 1964 - 1965 - 1966." Brussels.

Dutrieux, P., D. G. Vaughan, H. F. J. Corr, A. Jenkins, P. R. Holland, I. Joughin, and A. H. Fleming (2013), Pine Island glacier ice shelf melt distributed at kilometre scales, The Cryosphere, 7(5), 1543–1555, doi:10.5194/tc-7-1543-2013.

Favier, Lionel, Frank Pattyn, Sophie Berger, and Reinhard Drews. 2016. "Dynamic Influence of Pinning Points on Marine Ice-Sheet Stability: A Numerical Study in Dronning Maud Land, East Antarctica." The Cryosphere 10 (6). Copernicus GmbH: 2623–35. doi:10.5194/tc-10-2623-2016.

Frezzotti, Massimo, Stefano Urbini, Marco Proposito, Claudio Scarchilli, and Stefano Gandolfi. 2007. "Spatial and Temporal Variability of Surface Mass Balance near Talos Dome, East Antarctica." Journal of Geophysical Research 112 (F2): F02032. doi:10.1029/2006JF000638.

Helm, V, A Humbert, and H Miller. 2014. "Elevation and Elevation Change of Greenland and Antarctica Derived from CryoSat-2." The Cryosphere 8 (4): 1539–59. doi:10.5194/tc-8-1539-2014.

Holland, P. R., H. F. J. Corr, H. D. Pritchard, D. G. Vaughan, R. J. Arthern, A. Jenkins, and M. Tedesco (2011), The air content of Larsen Ice Shelf, Geophys. Res. Lett., 38(10), n/a-n/a, doi:10.1029/2011GL047245.

Jenkins, A., H. F. Corr, K. W. Nicholls, C. L. Stewart, and C. S. Doake (2006), Interactions between ice and ocean observed with phase-sensitive radar near an Antarctic ice-shelf grounding line, J. Glaciol., 52(178), 325–346.

Joughin, Ian. 2002. "Ice-Sheet Velocity Mapping: A Combined Interferometric and Speckle-Tracking Approach." Annals of Glaciology 34 (1). International Glaciological Society: 195–201.

Langley, K, A Deschwanden, J Kohler, A Sinisalo, K Matsuoka, T Hattermann, A Humbert, O A Nøst, and E Isaksson. 2014. “Complex Network of Channels beneath an Antarctic Ice Shelf.” Geophysical Research Letters 41 (4). Wiley Online Library: 1209–15.

Lenaerts, Jan, Joel Brown, Michiel R Van Den Broeke, Kenichi Matsuoka, Reinhard Drews, Denis and Callens, Morgane Philippe, et al. 2014. “High Variability of Climate and Surface Mass Balance Induced by Antarctic Ice Rises.” Journal of Glaciology 60 (224): 1101. http://www.staff.science.uu.nl/~lenae101/pubs/Lenaerts2014c.pdf.

Neckel, N., R. Drews, W. Rack, and D. Steinhage. 2012. “Basal Melting at the Ekström Ice Shelf, Antarctica, Estimated from Mass Flux Divergence.” Annals of Glaciology 53 (60): 294–302. doi:10.3189/2012AoG60A167.

Rignot, E., J. Mouginot, and B. Scheuchl. 2011a. “Ice Flow of the Antarctic Ice Sheet.” Science 333 (6048). American Association for the Advancement of Science: 1427–30. doi:10.1126/science.1208336.

Rignot, E., J. Mouginot, and B. Scheuchl. 2011b. “Antarctic Grounding Line Mapping from Differential Satellite Radar Interferometry.” Geophysical Research Letters 38 (10). Wiley Online Library. doi:10.1029/2011GL047109.

Shean, D. (2016), Quantifying ice-shelf basal melt and ice-stream dynamics using high-resolution DEM and GPS time series, Ph.D. Thesis, University of Washington, Seattle, WA, 14 July.

Shean, D. E., K. Christianson, K. M. Larson, S. R. M. Ligtenberg, I. R. Joughin, B. E. Smith, and C. M. Stevens (2017), In-situ GPS measurements of surface mass balance, firn compaction, and basal melt rates for the Pine Island Glacer Ice Shelf, Antarctica, The Cryosphere, submitted

Vaughan, David G, Hugh F J Corr, Robert A Bindschadler, Pierre Dutrieux, G Hilmar Gudmundsson, Adrian Jenkins, Thomas Newman, Patricia Vornberger, and Duncan J Wingham. 2012. “Subglacial Melt Channels and Fracture in the Floating Part of Pine Island Glacier, Antarctica.” Journal of Geophysical Research 117 (F3). Wiley-Blackwell. doi:10.1029/2012jf002360.

Detecting high spatial variability of ice-shelf basal mass balance (Roi Baudouin ice shelf, Antarctica)

Sophie Berger[1], Reinhard Drews[2], Veit Helm[3], Sainan Sun[1], and Frank Pattyn[1]

[1]Laboratoire de glaciologie, Université libre de Bruxelles, Brussels, Belgium
[2]Department of Geosciences, University of Tübingen, Tübingen, Germany
[3]Alfred Wegener Institute, Bremerhaven, Germany

Correspondence to: S. Berger (sberger@ulb.ac.be)

Abstract.

Ice shelves control the dynamic mass loss of ice sheets through buttressing and their integrity depends on the spatial variability of their basal mass balance (BMB), i.e., the difference between refreezing and melting. Here, we present ~~a novel~~ an improved technique – based on satellite observations – to capture the small-scale variability in the BMB of ice-shelves. As a case study, we apply the methodology to the Roi Baudouin Ice Shelf, Dronning Maud Land, East Antarctica and derive its yearly-averaged BMB at 10 m horizontal gridding. We use mass conservation ~~within~~ in a Lagrangian framework based on high-resolution surface velocities, atmospheric-model surface mass balance and hydrostatic ice-thickness fields (derived from TanDEM-X surface elevation). Spatial derivatives are implemented using the total-variation differentiation, which ~~avoids spatial averaging hence loss of spatial resolution~~preserves abrupt changes in flow velocities and their spatial gradients. Such changes may reflect a dynamic response to basal localised melting should be included in the mass budget. Our BMB field exhibits ~~high~~ much spatial detail and ranges from ~~-14.8~~ -14.7 to 8.6 m a^{-1} ice equivalent. Highest melt rates are found close to the grounding line where ~~the basal~~ pressure melting point is high, and the ice-shelf slope is ~~the steepest.~~ steep. The BMB field agrees well with on-site measurements from phase-sensitive radar, although independent radar profiling indicates unresolved spatial variations in firn density~~determined from profiling radar occur~~. We show that ~~the surface expression of an englacial lake~~ an elliptical surface depression (0.7×1.3 km ~~^{2} wide and 30~~wide and 10 m deep) lowers by 0.5 to 1.4 m a^{-1}, which we tentatively attribute to a transient adaptation to hydrostatic equilibrium. We find evidence for elevated melting beneath ice-shelf channels (with melting being concentrated on the channel's flanks). However, farther downstream from the grounding line, the majority of ice-shelf channels advect passively (i.e. no melting nor refreezing) toward the ice-shelf front. Although the absolute, satellite-based BMB values remain uncertain, we have high confidence in the spatial variability on sub-kilometre scales. This study highlights expected challenges for a full coupling between ice and ocean models.

1 Introduction

Approximately 74% of the Antarctic ice sheet is surrounded by floating ice shelves (Bindschadler et al., 2011a) providing the interface for interactions between ice and ocean. Marine ice sheets – characterized by a bed elevation below sea level and sloping down towards the interior – can be destabilised leading to a ~~Marine Ice Sheet Instability~~ marine ice sheet instability

(Mercer, 1978; Schoof, 2007; Tsai et al., 2015). However, ice shelves that are laterally constrained through embayments (or locally regrounded from below), mitigate the ~~Marine Ice Sheet Instability~~ marine ice sheet instability (Gudmundsson et al., 2012), thus regulating the ice flux from the inland ice sheet through buttressing. Over the last decade, major advances in our understanding of the processes at this ice-ocean interface have emerged, both theoretically (e.g. Pattyn et al., 2013; Favier et al., 2012, 2014; Ritz et al., 2015) as well as from observations (e.g. Rignot et al., 2014; Wouters et al., 2015). It is now established that ice-shelf integrity plays an important part in explaining sea-level variations in the past (Golledge et al., 2014; DeConto and Pollard, 2016), enabling improved projections of future sea-level rise (Golledge et al., 2015; Ritz et al., 2015).

~~While oceanic processes play a dominant role in ice-shelf basal mass balance, ice-shelf~~ Ice-shelf integrity can be ~~further~~ compromised by atmospheric driven surface melt-ponding (Lenaerts et al., 2017) and hydrofracturing (Banwell et al., 2013; Scambos et al., 2004; Hulbe et al., 2004). From the ocean side, ice shelves may thin or thicken (Paolo et al., 2015) due to changes in basal mass balance (BMB), i.e. the difference between refreezing and melting. Point measurements with phase-sensitive radars (Marsh et al., 2016; Nicholls et al., 2015), global navigation satellite system (GNSS) receivers (Shean et al., 2017) , observations from underwater vehicles (Dutrieux et al., 2014) and analysis from high-resolution satellites ~~(Dutrieux et al., 2013)~~ (Dutrieux et al., 20 shown that ~~the~~ BMB varies spatially on sub-kilometre scales. Ice-shelf channels are one expression of localised basal melting (Stanton et al., 2013; Marsh et al., 2016) which~~forms curvilinear tracts in ice shelves where ice is more than 50 thinner than its surrounding~~ , after hydrostatic adjustment, form curvilinear depressions visible at the ice-shelf surface (Fig. 1). These surface depressions virtually always reflect basal incisions resulting in curvilinear tracts of thin ice. In some areas, ice-shelf channels are twice as thin as their surroundings (Drews, 2015). However, the impact of ice-shelf channels on ice-shelf integrity is yet unclear because, on the one hand, excessive basal melting beneath ice-shelf channels may prevent ice-shelf-wide thinning (Gladish et al., 2012; Millgate et al., 2013) but, on the other hand, increased crevassing due to channel carving may structurally weaken the ice shelf (Vaughan et al., 2012).

Here we attempt to derive the BMB of the Roi Baudouin Ice Shelf (RBIS), Dronning Maud Land, East Antarctica, at 10 m gridding, based on mass conservation in a Lagrangian framework. The RBIS (Fig.~~4~~1) is constrained by an ice promontory to the West and by Derwael Ice Rise in the East, blocking the tributary flow from Western Ragnhild Glacier ~~,~~ one of the largest outlet glaciers in Dronning Maud Land (Callens et al., 2014). ~~Analysis~~ Analyses on Derwael Ice Rise (Drews et al., 2015; Callens et al., 2016) and the larger catchment area (Favier et al., 2016) suggest that the RBIS is a relatively stable sheet-shelf system on millennial time scales. The RBIS contains a number of ice-shelf channels (Drews, 2015, and arrows in Fig. 2e), many of which start at the grounding line and extend over 230 km ~~all the way~~ to the ice-shelf front.

~~In the following, we~~ We outline our approach of deriving the BMB, with ~~a special~~ focus on attaining high spatial resolution~~results~~. Resolving BMB is challenging, because it is computed as the residual of ~~large numbers~~ several uncertain quantities and it relies on spatial derivatives, which amplify noise in the input data. The latter can be accounted for with spatial averaging (e.g. Neckel et al., 2012; Moholdt et al., 2014), which, however, may smear out the processes acting on sub-kilometre scales. Here, we use spatially well-resolved input data combined with total-variation regularization of the velocity gradients. This avoids spatial averaging, but still ~~accounts for~~ mitigates the noise in the input data. As a result, our BMB field shows high detail over different spatial scales that are validated with phase-sensitive ~~and ground-penetrating radarobservational evidence,~~

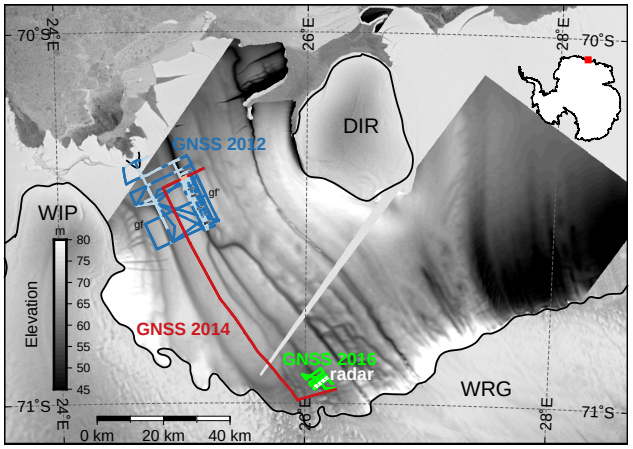

Figure 1. Overview of the topography of the Roi Baudouin Ice Shelf (from TanDEM-X 2014) and ground-truth datasets presented and discussed in the text (Sect 2.7 and 4). Acronyms stand for DIR: Derwael Ice Rise, WIP : Western Ice Promontory and WRG: West Ragnhild Glacier. The profile gf-gf' is shown in Fig. S2. Light blue and light red are the low-lying parts of the ice-shelf, which are excluded from the GNSS-TanDEM-X comparison in Fig. 9. "Radar" denotes both ground-penetrating and phase sensitive radars. The background is from the Radarsat mosaic (Jezek and RAMP-Product-Team, 2002) and the black line delineates the grounding line (Depoorter et al., 2013) .

~~as well as kinematic global navigation satellite system (GNSS) profiling~~radar, GNSS observations and ground-penetrating radar.

~~Lagrangian Basal Mass Balance (LBMB) of the Roi Baudouin Ice Shelf. Red and blue colours indicate basal melting and refreezing, respectively. Insets (a), (b) and (c) locate the close-ups presented in figures 6, 7 and 3. Labels 1-3 pinpoint areas discussed in the text. Acronyms stand for DIR: Derwael Ice Rise, WIP : Western Ice Promontory and WRG: West Ragnhild Glacier. The LBMB overlays the 2014 TanDEM-X DEM in slight transparency. The background is from the Radarsat mosaic (Jezek and RAMP-Product-Team, 2002) and the black line delineates the grounding line (Depoorter et al., 2013) .~~

2 ~~Method~~Data and methods

2.1 Basal mass balance from mass conservation

We ~~derived~~ derive the basal mass balance ($\dot{M}_b$) from mass conservation, i.e.,

$$= \frac{\partial H}{\partial t} + \nabla \cdot (H\boldsymbol{u}) - \dot{M}_s = \frac{\partial H}{\partial t} + (\boldsymbol{u} \cdot \nabla H + H \nabla \cdot \boldsymbol{u}) - \dot{M}_s = \frac{\mathrm{D}H}{\mathrm{D}t} + H\,(\nabla \cdot \boldsymbol{u}) - \dot{M}_s$$

(

$$\dot{M}_b = \frac{\partial H_i}{\partial t} + \nabla \cdot (H_i \boldsymbol{u}) - \dot{M}_s \tag{1a}$$

$$= \frac{\partial H_i}{\partial t} + (\boldsymbol{u} \cdot \nabla H_i + H_i \nabla \cdot \boldsymbol{u}) - \dot{M}_s \tag{1b}$$

$$= \frac{\mathrm{D}H_i}{\mathrm{D}t} + H_i (\nabla \cdot \boldsymbol{u}) - \dot{M}_s \tag{1c}$$

where $\dot{M}_s$ is the surface mass balance (SMB, positive values for mass gain), ~~H~~ H_i is the ice thickness and $\boldsymbol{u}$ the ~~vertically-integrated horizontal ice velocity~~ column-average horizontal velocity of the ice. $\dot{M}_b$, $\dot{M}_s$ and ~~H~~ H_i are given in ice-equivalent units. ~~In principle eq~~$\partial H_i/\partial t$ and $\mathrm{D}H_i/\mathrm{D}t$ represent the Eulerian and Lagrangian thickness change, respectively and $\nabla \cdot (H_i \boldsymbol{u})$ denotes the flux divergence, that includes advection of thickness gradients ($\boldsymbol{u} \cdot \nabla H$) and ice-flow divergence ($H_i \nabla \cdot \boldsymbol{u}$). In principle, Eq. (1) does not depend on the reference frame and can be calculated in both a fixed coordinate system (i.e. Euler coordinates) or with a moving coordinate system that follows the ice flow (i.e. Lagrange coordinates). In practice, however, both approaches differ~~greatly: an Eulerian coordinate system requires only~~ : Eulerian studies are often based one thickness field ~~in time and typically accounts~~ and either assume steady-state (Rignot and Steffen, 2008; Neckel et al., 2012) or rely on an external dataset (Depoorter et al., 2013; Rignot et al., 2013) to account for the thickness ~~change $\partial H/\partial t$ explicitly (Depoorter et al., 2013; Rignot et al., 2013) or assumes a steady-state (Rignot and Steffen, 2008; Neckel et al., 2012)~~ changes $\partial H_i/\partial t$ (e.g. Pritchard et al., 2012; Paolo et al., 2015) . The Lagrangian approach, ~~however~~on the other hand, requires two thickness fields covering different time periods from which the Lagrangian thickness change is calculated implicitly (~~$\mathrm{D}H/\mathrm{D}t$~~$\mathrm{D}H_i/\mathrm{D}t$). As shown below, the key difference between both approaches is how the advection of thickness gradients ($\boldsymbol{u} \cdot \nabla H$) is accounted for. ~~In~~ The Lagrangian approach is best-suited in areas where advection is significant (e.g. near ice-shelf channels)~~, this can only be adequately done in a Lagrangian framework~~. We refer to previous publications ~~(Dutrieux et al., 2013; Moholdt et al., 2014)~~ (Dutrieux et further explain differences between Eulerian and Lagrangian approaches.

~~We~~ In the following, we describe surface velocities in ~~section 2.2, SMB in section 2.3and~~ Sect. 2.2, surface mass balance in Sect. 2.3, the derivation of hydrostatic ice thickness in ~~section 2.4~~ Sect. 2.4 and Lagrangian thickness change in Sect. 2.5. Key features of the input datasets are summarised in Table1. As a novelty compared to previous studies, we base our hydrostatic thickness field on high-resolution digital elevation models (DEMs) derived from TanDEM-X images ~~of~~ from 2013 and ~~2014, clearly resolving ice-shelf channels.~~ 2014. Section 2.6 explains the implementation of spatial velocity gradients ($\nabla \cdot \boldsymbol{u}$ in ~~eq~~Eq. (1)), which is non-trivial when derivatives are taken over short distances with noisy input data. We ~~calculate the Lagrangian thickness change $\mathrm{D}H/\mathrm{D}t$ by cross-correlating the TanDEM-X DEMs (using 5×5 km^2 patches and a normalized cross-correlation threshold of 0.8). We also investigate an alternative approach of using the observed surface velocities to shift the thickness field (Moholdt et al., 2014, and section 4) .~~

~~We~~ compare the derived Lagrangian Basal Mass Balance (LBMB) with field measurements of phase-sensitive radar and GNSS profiling (~~section~~ Sect. 2.7). Although this is not a direct validation, as the field data cover a different period, the comparison is insightful to understand the spatial variability in our LBMB field. The derived LBMB is only valid in freely floating

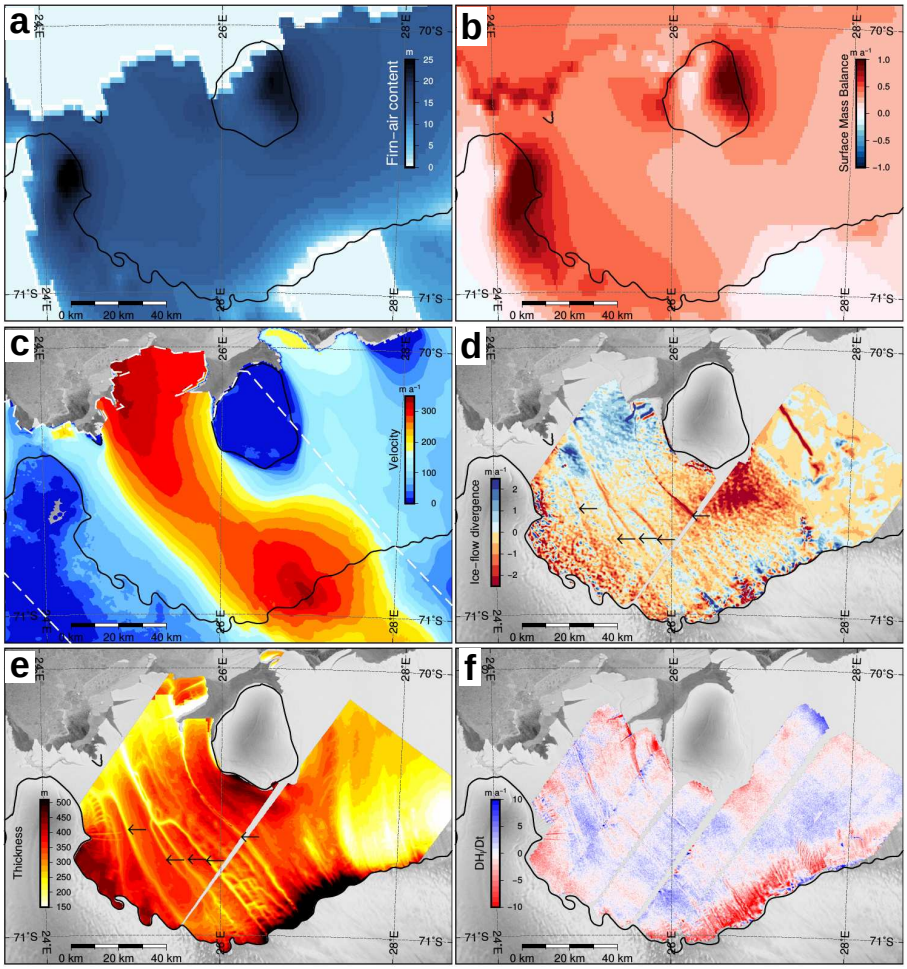

Figure 2. (a, c, e) Variables entering Eqs. (1) and (2) and (b, d , f) terms needed to calculate the LBMB in Eq. (1). (a) Firn-air content (H_a); (b) surface mass balance ($\dot{M}_s$); (c) surface velocities ($\boldsymbol{u}$) (the white dashed line delinates the flow field from Berger et al. (2016)); (d) ice-flow divergence (~~$H(\nabla \cdot \boldsymbol{u})$~~$H_i(\nabla \cdot \boldsymbol{u})$) (Note: the red band 30km east of Derwael ice rise is caused by a seam in Rignot et al. (2011b) 's flow field); (e) hydrostatic ice thickness of 2014 (~~H~~H_i) and (f) Lagrangian thickness change (~~DH/Dt~~$\mathrm{D}H_i/\mathrm{D}t$). Arrows in (d) and (e) locate ice-shelf channels. The background is from the Radarsat mosaic (Jezek and RAMP-Product-Team, 2002) and the black line delineates the grounding line (Depoorter et al., 2013). Key features regarding the input datasets are summarised in Table 1.

areas, which excludes the grounding zone, but also other small-scale features such as ~~viscous inflow in~~ ice-shelf channels ~~(Humbert et al., 2015; Drews, 2015) .~~ where viscous inflow can occur (Humbert et al., 2015; Drews, 2015) . (Examples where this may be the case are discussed in ~~section 5~~Sect. 5).

2.2 Surface velocities from satellite radar remote sensing

~~We~~ Assuming that velocities do not vary with depth, we use surface velocities that were previously derived by combining interferometric Synthetic Aperture Radar (InSAR) and speckle tracking (Berger et al., 2016). The velocities are mosaicked and gridded to a 125 m posting and are based on images from the European Remote Sensing satellites (ERS 1/2) ~~of~~ from 1996 and the Advanced Land Observing System Phased Array type L-band Synthetic Aperture Radar (ALOS-PALSAR) ~~of~~ from 2010. ~~Comparison~~ As shown in Berger et al. (2016) , comparison with on-site ~~GNSS~~ measurements collected in ~~2014~~ 1965-1967 and 2012-2014 yields no evidence ~~for temporal variations in the yearly averaged ice velocities . This dataset~~ of prominent changes in the ice velocities over the last decades, which supports the combination of data from different dates. The velocity mosaic covers 75% of our area of interest (dashed line in Fig. 2c). The remaining areas are filled ~~in~~ with an Antarctic-wide flow field (Rignot et al., 2011b) gridded to ~~a~~ 900 m ~~posting~~ postings (the 450 m gridded velocities ~~being~~ are too noisy in our area of interest). We reduce ~~cutting edges~~ seams – as high as 60 m a^{-1} in some places – using linear feathering (e.g. Joughin, 2002; Neckel et al., 2012) over 4.5 km.

2.3 Surface mass balance from atmospheric modelling

~~The SMB is based on~~ We use the surface mass balance from a high-resolution (5.5 km posting) simulation of the Regional Atmospheric Climate MOdel (RACMO) version 2.3, centred on Dronning Maud Land (25 °W and 45°W) and ~~spanning~~ averaged over the period 1979–2015 (Lenaerts et al., 2014, 2017). The SMB field correctly reproduces asymmetries across Derwael Ice Rise originating from orographic uplift and also ~~predicts~~ simulates a corresponding shadowing effect on the Roi Baudouin Ice Shelf (Fig. 2b and Lenaerts et al., 2014) . Moreover, the simulation explains observed surface melting near the grounding zone due to a wind-albedo feedback caused by persistent katabatic winds in this area (Lenaerts et al., 2017).

2.4 Hydrostatic Ice Thickness

We calculate the ice thickness (Fig. 2e) by imposing hydrostatic equilibrium on surface freeboard (Bindschadler et al., 2011b; Chuter and Bamber, 2015; Drews, 2015) ~~. The DEMs were~~ derived from the TanDEM-X satellites. The details of hydrostatic inversion are presented in the following two sections.

Surface elevations

The digital elevation models are processed from 43 image pairs (Fig. S1) of the TanDEM-X mission ~~. The~~ (Krieger et al., 2007) , in which the TerraSAR-X and ~~TandDEM-X~~ TanDEM-X satellites image the surface simultaneously from different viewing angles~~, hence allow inferring the~~ . This allows to infer topography interferometrically without the need to correct for ice flow. Images from the austral winters of 2013 and 2014 are processed to single-look complex scenes, using SARscape®. After coregistration using the CryoSat-2 DEM (Helm et al., 2014), the pairs are differenced in phase. The resulting interferograms are then unwrapped and the phase difference is re-flattened before being geo-referenced in polar stereographic coordinates. The processing provides 43 single DEMs (32 from 2013 and 11 from 2014) gridded to 10 ~~m with an estimated relative vertical accuracy better than 1 m(based on the standard deviation in overlapping areas). DEMs~~ m. They cover a time span ranging

from 21/06/2013 to 10/07/2014 (Fig. S1). The maximum temporal difference at overlapping areas between the 2013 and 2014 DEMs is 379 days.

Digital elevation models from the same date and satellite path are concatenated together, with a linear taper on overlapping zones. Grounded areas are masked out using the composite grounding line from Depoorter et al. (2013). DEMs based on SAR interferometry can exhibit a flawed elevation trend due to imprecise information about the satellite orbits or due to parameter estimation , based on differential InSAR with Radarsat and PALSAR (Rignot et al., 2011a) at RBIS. To correct for small elevation shifts between the different frames, which we assume uniform over the ice shelf, we tie the 2013 concatenated frames to each other and to the CryoSat-2 DEM (Helm et al., 2014) , using constant offsets. We attribute this small shifts to tides, inverse barometric effect or different calibration during the SAR processing(Drews et al., 2009) . In our case, this is evident in the .

All DEMs are smoothed with a Gaussian filter to remove small-scale surface roughness. The standard deviation of the filter is set to 7 pixels (or 70 m) in all directions. This means that points lying within that distance are weighted with 0.68. To determine the size of the Gaussian filter, we investigated standard deviations from 1-10 pixels and found that using 7 pixels minimises the elevation discrepancy between 2012 GNSS and TanDEM-X surface elevation (Sect. 2.7). As shown in Fig. S2, the applied smoothing does not affect the shape of the surface depressions linked to ice-shelf channels (with a typical width of 1-2 km).

The difference fields of the individual DEMs , which 2013-2014 overlapping DEMs exhibit a linear trend aligned with the satellite trajectory. We correct for this by fitting a plane to the difference field that is subtracted from the attribute this signal to the interferometric processing, which can leave a flawed elevation trend due to imprecise information about the satellite orbits or due to ill-constrained parameters during the SAR processing (Drews et al., 2009) . To account for this effect, we subtract a plane from the 2014 DEMs. This adjustment is further discussed in section 4. Additionally, all DEMs are smoothed with a Gaussian filter removing small-scale surface roughness. The standard deviation of the Gaussian filter was set to 7, because it minimizes the mean and standard deviation of the difference between the DEM using the difference fields of 2013-2014 overlapping fields. The plane fit and the offset correction applied earlier mask absolute $\partial H_i/\partial t$ changes, which we assume to be small in the following.

To assess the relative vertical accuracy of the final DEMs (Sect. 4.1) (i) we use the difference fields of overlapping, unconcatenated TanDEM-X DEMs and GNSS profiles collected on-site. The frames from the same date and satellite path (Fig. S3), and (ii) we compare the DEMs to kinematic GNSS profiling. We estimate the relative vertical accuracy to be better than 1 m, although elevation differences in some areas are systematically higher (Sect 2.7). The offset and plane fitting corrections are further discussed in Sect. 4.1, as they strongly impact the quality of our ice-thickness fields and the resulting BMB rates, strongly depend on the corrections applied here, which is further discussed in section 4. LBMB rates.

We apply the hydrostatic equilibrium on

Hydrostatic equilibrium

We invert hydrostatic thickness from freeboard heights (h_{asl}) with densities of ~~$\rho_w = 1027\ kg\ m^{-3}$, $\rho_i = 910\ kg\ m^{-3}$ and $\rho_a = 2\ kg\ m^{-3}$~~ ρ_w=1027 kg m^{-3}, ρ_i=910 kg m^{-3} and ρ_a=2 kg m^{-3}, for seawater, ice and firn air, respectively :

$$H_i = \frac{\rho_w h_{asl}}{\rho_w - \rho_i} - \frac{H_a(\rho_w - \rho_a)}{\rho_w - \rho_i}. \tag{2}$$

The firn-air content H_a accounts for the ~~variable firn density~~ lower firn and snow densities by subdividing the ice column in air- and ice-equivalent layers. We use simulated values from the firn-densification model 'IMAU-FDM' ~~(Ligtenberg et al., 2011; Lenaerts et al.,~~ which is forced by the SMB~~and~~ , exists on the same spatial grid (5.5 km, ~~section 2.3)~~ Sect. 2.3) and is averaged over the same time-period (1979-2015). For converting ellipsoidal heights to freeboard elevations we employ the EIGEN-6C4 geoid (Förste et al., 2014) and the DTU12MDT mean dynamic topography model (Knudsen and Andersen, 2012). The hydrostatic ice thickness is most sensitive to the firn-air content and the freeboard ~~height~~heights, resulting in an estimated uncertainty of at least $\pm$ 25 m (Drews, 2015). However, as discussed ~~below~~in Sect. 4.1, uncertainties can be much higher in areas where firn density is ill-constrained.

2.5 ~~Spatial derivatives with noisy input data~~Lagrangian thickness change

As Lagrangian frameworks move with the flow, computing the Lagrangian thickness change $\mathrm{D}H_i/\mathrm{D}t$ requires to shift one thickness field to match the geometry of the second one. Consequently, this approach implicitly accounts for advection of thickness gradients ($\boldsymbol{u} \cdot \nabla H_i$). Here, the 2013 TanDEM-X frames are shifted forward with a normalized correlation-coefficient matching algorithm from the computer vision library OpenCV (Bradski and Kaehler, 2008) . Each 2013 concatenated frame is divided in 5×5 km patches that are sampled every kilometre in both directions. Each 2013 patch is then compared with any possible 5×5 km patch within a slightly bigger search region (6.6×6.6 km) in the 2014 DEMs that overlap with the 2013 DEM. Comparison is based on normalized cross-correlation coefficients technique, a more robust variant of 2D normalised cross correlation (Marengoni and Stringhini, 2011) . The shift of the 2013 patches is found where the correlation coefficient is maximum. Mismatches are discarded when the correlation-coefficient is smaller than 0.8, or when the detected offset is well beyond what would be expected from the available flow-field. All the 2013 shifted patches are then mosaicked to construct a shifted 2013 frame that matches the geometry of its overlapping 2014 frame. The process is applied to each overlapping pair of 2013-2014 TandDEM-X frames before conversion to hydrostatic thickness.

In Sect. 4.1, we investigate an alternative approach using observed surface velocities to shift the DEMs with a 10 day time-step (as in Moholdt et al., 2014) . We also apply this alternative approach to shift the 2016 GNSS profiles (Sects. 2.7, 3.2 and 5).

2.6 Spatial derivatives of noisy input data

Taking spatial gradients in ~~eq~~Eq. (1) is not straightforward as naive discretization schemes (e.g. forward, backward or central differences) greatly amplify the signal-to-noise ratio if the input data are noisy. ~~Although this is typically~~ This can be accounted for by smoothing the input data (e.g. Moholdt et al., 2014) and/or by increasing the lateral distances over which the derivative is approximated (e.g. Neckel et al., 2012)~~, it is largely unsuited to resolve small-scale features such as ice-shelf channels.~~

~~Smoothing the surface velocities with a kernel comparable to the size of~~ . However, smoothing prior to taking the derivative can lead to smearing out of the derivative in areas where the derived quantity changes abruptly (or discontinuously). We expect such abrupt changes in the surface velocities across ice-shelf ~~channels subdues small-scale anomalies in the flow field (e.g. lateral convergence), which can accompany locally elevated basal melt rates (Drews, 2015)~~ . channels that experience strong basal melting (Drews, 2015) . To circumnavigate this problem, we applied the total-variation regularization, ~~which formulates the derivative as an inverse problem, and where the wiggliness of the derivative is controlled through~~ a technique that suppresses noise from spatial derivatives while preserving abrupt changes (Chartrand, 2011) . Noise is removed from the data by reducing the total variation of the signal to a certain degree controlled by a regularization parameter α (Chartrand, 2011). ~~By exploring~~ The α ~~values ranging from 1 to 10^6, the value of~~ value we use (10^5 ~~was retained as the best trade-off between noise reduction and loss of small-scale variability. Fig. 3 compares a regularized derivative with a derivative based on central differences and smoothed input data, which we discuss in section 4. This α value was chosen considering the standard deviation between the observed and regularized velocities (resulting from the integration of the regularized derivatives). $\alpha = 10^5$ results in a standard deviation of 4.5 m/a at the centre of our area of interest, which approximately corresponds to our estimated error in the velocities and suggests that with this alpha the regularization successfully suppresses the noise while keeping the signal. However,~~) is given by the variance of the velocities, following the discrepancy principle (Chartrand, 2011) . Figure 3 compares regularized derivatives with derivatives based on velocity fields that were smoothed to varying degrees prior to taking the derivatives using central differences. It should be noted that some ambiguity about the specific choice of α remains ~~, which~~ but this is inherent to regularization in general. We discuss the benefits and trade-offs of the different derivative schemes further in Sect. 4.2.

2.7 On-site geophysical measurements

~~During the Austral winter of 2015-2016,~~ Remote-sensing and modelling data are complemented by a series of geophysical measurements ~~were carried out on the RBIS, such as~~ (ground-penetrating radar, GNSS profiling and phase-sensitive radar measurements) carried out in December 2012, December 2014 and January 2016 (Fig. 1).

The ground-penetrating radar profile shown in Fig. 8a ~~was acquired~~ (located in Fig. 1) was acquired in 2016 with a 20 MHz pulsed radar (Matsuoka et al., 2012). The data ~~were~~ are geolocated with kinematic GNSS and migrated using Kirchoff-depth migration with a velocity-depth function that accounts for the low firn-air content in this area. More details about acquisition and processing of the radar data are given in Drews et al. (2015). We use the radar ice thickness to validate the hydrostatic ice thickness (~~section 4~~Sect. 4.1).

~~The~~

We use three sets of kinematic GNSS profiles that were recorded at 1 Hz intervals with geodetic, multi-channel receivers moving at a speed below 12 km h^{-1}. ~~The data were processed differentially, relative to a non-moving base station (Drews et al., 2015) . Elevations were~~ In December 2012, a 20×25 km GNSS network was acquired at the front of the ice shelf (Drews, 2015) . The profiles cross ice-shelf channels multiple times. Two years later in December 2014, a 100 km-long North-South GNSS transect was acquired (Lenaerts et al., 2017) . The last GNSS dataset was acquired in January 2016, along and across an elliptical surface depression (Sect 3.2). All GNSS elevations are de-tided using the circum-Antarctic tide model (CATS2008a_opt)

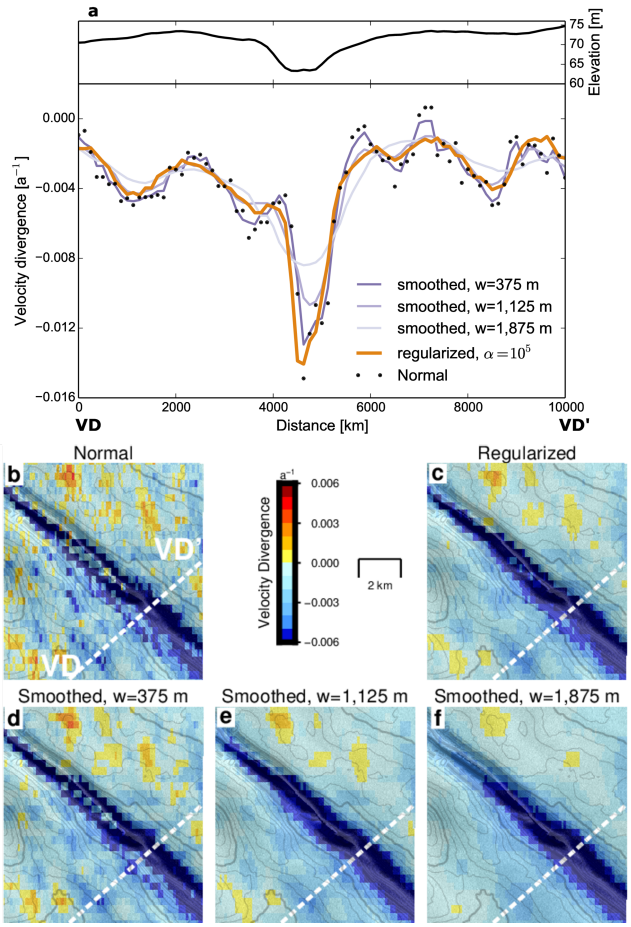

Figure 3. Velocity divergence at an ice-shelf channel located in Fig 4. (a) Profile showing elevation and velocity divergence for various degree of smoothing (w = window width) and after regularization ($\alpha = 10^5$). (b -f) corresponding spatial pattern of the velocity-divergence profiles shown in (a) . The background image is from Landsat 8, acquired in 2014 and the maps are overlain with elevation contour lines of 1 m.

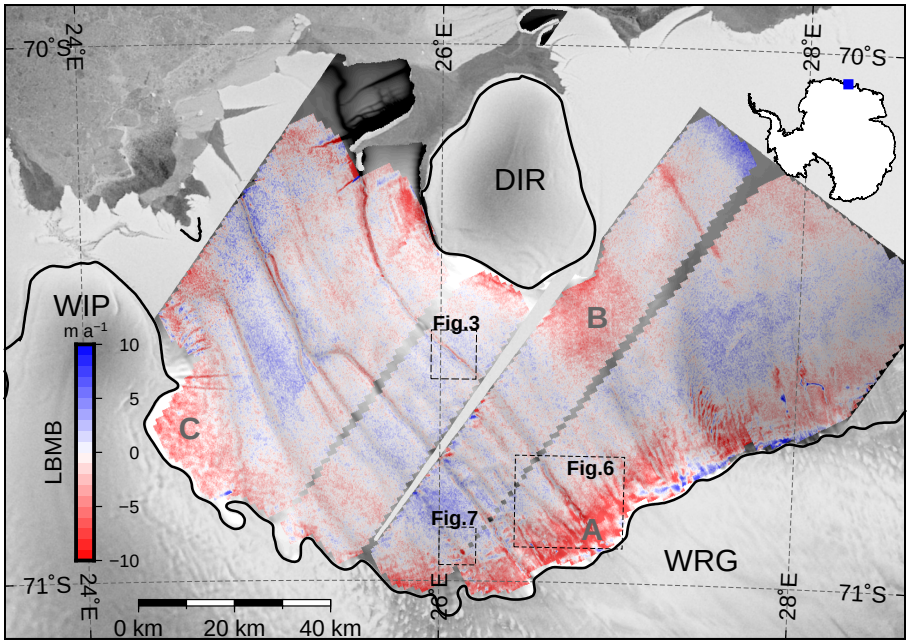

Figure 4. ~~Eulerian~~ Lagrangian Basal Mass Balance ~~in steady state~~ ($\partial H/\partial t = 0$LBMB) of the Roi Baudouin Ice Shelf. Red and blue colours indicate basal melting and refreezing, ~~overlaying~~ respectively. The 3 dashed boxes locate the close-ups presented in Figs. 3, 6 and 7. Labels A-C pinpoint areas discussed in the text. Acronyms stand for DIR: Derwael Ice Rise, WIP : Western Ice Promontory and WRG: West Ragnhild Glacier. The LBMB overlays the 2014 TanDEM-X DEM~~in slight transparency~~. The background is from the Radarsat mosaic (Jezek and RAMP-Product-Team, 2002) and the black line delineates the grounding line (Depoorter et al., 2013).

from Padman et al. (2002, 2008). ~~The same data is used~~ Datasets from 2012 and 2016 are processed differentially, relative to a non-moving base station (Drews et al., 2015) , while data from 2014 are post-processed with Precise Point Positioning. Elevations from GNSS are used (i) to determine the size of the Gaussian filter applied to the TanDEM-X DEMs (2012 survey, Sect. 2.4), (ii) to assess the accuracy of the TanDEM-X DEMs (2012 and 2014 surveys, Sect. 4.1) and (iii) to extend the time period of surface elevation change detected by the TanDEM-X mission (2016 survey, Sect. 3.2 and 5; Figs. 7 and 8).

BMB was measured at point locations using a phase-sensitive radar. Processing and acquisition schemes are as outlined previously (Nicholls et al., 2015; Marsh et al., 2016). The radar antennas were positioned at 22 sites. Each site was remeasured after 10 days at ~~exactly~~ the same location at the surface (in a Lagrangian framework). This way, relative thickness changes due to strain thinning and basal melting can be detected within millimetres. Strain thinning is corrected using a linear approximation of the vertical strain rate with depth, based on tracking the relative displacement of internal reflectors. The strain correction of the BMB rates is small (6.6×10^{-3} ~~m~~ a^{-1} on average), because strain thinning ~~in the 10-day interval is smallcompared to the inferred basal melt rates, i.e., approximately 1.1 m a^{-1}~~is small.

3 Results

3.1 Large-scale pattern of the Basal mass balance

The LBMB rates range from ~~-14.8~~ -14.7 to 8.6 m a^{-1} (excluding outliers with 0.1 and 0.99 percentiles) and average -0.8 m a^{-1} (negative values signify melting, positive values refreezing). ~~Fig. 4 shows that most~~ For the area covered by the TanDEM-X DEMs, net mass loss at the ice-shelf bottom is 6.7 Gt a^{-1}. Most melting occurs just ~~seawards~~ seaward of the grounding zone where the western Ragnhild Glacier feeds into the Roi Baudouin Ice Shelf (~~label 1~~Fig. 4, label A). This area corresponds to the thickest and fastest part of the grounding zone (Fig. 2e and c). We also find elevated melting close to the western ice promontory (~~label 2~~Fig. 4, label C) and on the ~~stoss~~ southern side of Derwael Ice Rise (~~label 3).~~ Fig. 4, label B).

The uncertainties of the absolute LBMB are typically higher than the LBMB itself, because errors unfavourably propagate in mass budgets (Moholdt et al., 2014). Here, we assess a lower bound of the LBMB errors by using the difference fields of the individual LBMB frames in overlapping areas. These show no systematic patterns and the standard deviation amounts to 2.3 m a^{-1}. Moreover, comparing the (yearly averaged) LBMB values with the 22 on-site ~~, 10-day averaged~~ phase-sensitive radar measurements, reveals differences of 1.1±2.6 m a^{-1} in mean and standard deviation, respectively. ~~Qualitatively,~~ We discuss this comparison in more detail in Sect. 3.2. Figures 2b,d,f illustrate the terms entering Eq. (1c), namely surface mass balance, ice-flow divergence and Lagrangian thickness change, whereas Figs. 2a,c,e display the most critical input variables needed to compute those different terms, i.e., firn-air content, ice velocity and hydrostatic thickness. For the RBIS, the Lagrangian thickness change dominates the BMB (as in Shean et al., 2017) , while ice-flow divergence and SMB are both one order of magnitude lower. Qualitatively the large-scale pattern agrees well with the results from Rignot et al. (2013) who also found the highest melt rates close to the grounding line, both for steady state or transient approximations. ~~To demonstrate the necessity~~

To illustrate the advantages of the Lagrangian approach, ~~we also calculate the BMB in a steady-state Eulerian framework. As shown~~ Fig. 5 shows the Eulerian thickness change, flux divergence and Eulerian BMB. While the large-scale pattern of the Eulerian BMB agrees very well with that of the LBMB, the Eulerian approach fails in the vicinity of ice-shelf channels (arrows in Fig. ~~??, this~~ 5). Advecting topographic features imprint the Eulerian thickness changes (Fig. 5a), however, the Eulerian approach does not fully account for this advection of thickness gradients ($\boldsymbol{u} \cdot \nabla H_i$) in the flux divergence (Fig. 5c). This results in spurious ~~signals in particular close to~~ Eulerian BMB in the vicinity of ice-shelf channels ~~, due to advection of thickness gradients ($\boldsymbol{u} \cdot \nabla H$)that are not adequately accounted for. A high-resolution, transient version of the Eulerian thickness change is difficult, because the~~ (Fig. 5c). These spurious signals in the Eulerian BMB become even stronger when thinning/thickening rates ~~($\partial H/\partial t$) have to be prescribed~~ are taken from external datasets ~~, which are typically not~~ which are spatially less well resolved. Using ice-shelf wide, average values (e.g. repeat satellite altimetry) does not account for the advection of ice-shelf channels and other (transient) features in the ice-shelf, hence ~~violating the steady-state assumption~~introducing artifacts in the basal mass balance pattern.

~~Figs. 2b,d,f illustrate the terms entering Eq. (1), i.e., SMB, ice-flow divergence and Lagrangian thickness change, whereas Figs. 2a,c,e display the most critical input variables needed to compute those different terms, i.e., firn-air content, ice velocity~~

~~and hydrostatic thickness. For the RBIS, the Lagrangian thickness change dominates the BMB (as in Shean et al., 2017) , while the ice-flow divergence and the SMB are both one order of magnitude lower.~~

3.2 Small-scale variability

The larger scale ~~BMB~~ LBMB pattern (>10 km) is overlain by smaller-scale variability. Ice-shelf channels appear most clearly in the DEMs and thus in the hydrostatic thickness fields (arrows in Fig. 2e). ~~To a lesser extent~~In some places, they also co-locate with areas of lateral inflow (i.e., negative flow divergence; arrows in Fig. 2d) and Lagrangian thinning (i.e., negative Lagrangian thickness change in Fig. 2f). In the LBMB, ice-shelf channels appear partially as narrow bands of intense melting~~(e.g. insets a and b in Fig. 4). Fig.~~ . Figure 6 shows one example where ice preferentially melts at the flanks of an ice-shelf channel. LBMB rates drop to ~~-5m~~-5 m a^{-1} at both flanks, whereas outside the channel ~~and at the channel's apex , the LBMB is close to zero~~the LBMB is close to zero. The slight refreezing found at the channel's apex (1.5 m a^{-1}) is very close to the detection limit and its magnitude is 3 times lower than what is observed at the flanks.

Another example of a small-scale feature is illustrated in Figs. 7 and 8. Here, we observe a 0.7×1.3 km ^{2} ~~ellipsoidal surface depression which is connected to~~ elliptical surface depression that is up to 10 m lower than its surroundings and located on the upstream end of an ice-shelf channel~~on its downstream end (Fig 7a)~~. The surface topography also exhibits secondary elongated surface depressions that ~~merge like tributaries into the ellipsoidal depression(marked with arrows in Fig. 7).~~ are shaped like fingers merging into the elliptical depression. We surveyed this area in 2016 with kinematic GNSS profiles~~of~~ , ground-penetrating radar and 22 point-measurements of the ~~LBMB~~ BMB with phase-sensitive radar (~~section~~ Sect. 2.7). Lenaerts et al. (2017) identified this feature as one of the 55 ~~englacial lakes~~ features on the Roi Baudouin Ice Shelf, that can be linked to the formation of englacial lakes near the grounding line. They proposed that these ~~lakes are at first~~ features are initially formed as supra-glacial ~~and form~~ lakes in the grounding zone due to katabatic wind-albedo feedback. Freezing at the lake surface and subsequent burial by snowfalls form ~~the~~ at first englacial lakes that are advected farther downstream. ~~In this case, the hypothesized water-ice interface is~~ As a function of the advection time the liquid water then likely fully refreezes. For the elliptical surface depression considered here, the radar data show a bright reflector at approximately 30 m depth and ~~blocks the penetration of radar waves~~ no coherent signals appear at larger depths (Fig. 8a). ~~With today's surface velocities, it would require ~50 years for the lake to be advected from the grounding line to its current position. We have no direct evidence for an englacial lake at this location and it is also possible that radar penetration is blocked by some other internal, specular reflector (such~~ We tentatively interpret the bright radar reflector as a refrozen surface of a former ~~lake). The specifics~~ supra-glacial lake. The specularity of this interface ~~, however, are not important here as we focus exclusively on its surface expression. The englacial lake area~~ hinders deeper penetration of the radar signal. However, a more detailed radar analysis is warranted to unambiguously clarify the origin and history of this feature. Here, we restrict ourselves to the elliptical surface depression where we observe significant surface lowering.

The elliptical depression appears prominently in our LBMB field with rates ~~down to~~ as low as -12 m a^{-1} (Figs. ~~8b and 7~~7b and 8b). ~~Outside the englacial lake area~~On the eastern side of the depression, the BMB from the phase-sensitive radar (Fig. 8b) agrees well with the LBMB estimate~~. On the eastern side, we find a near-perfect fit with~~ , both methods averag-

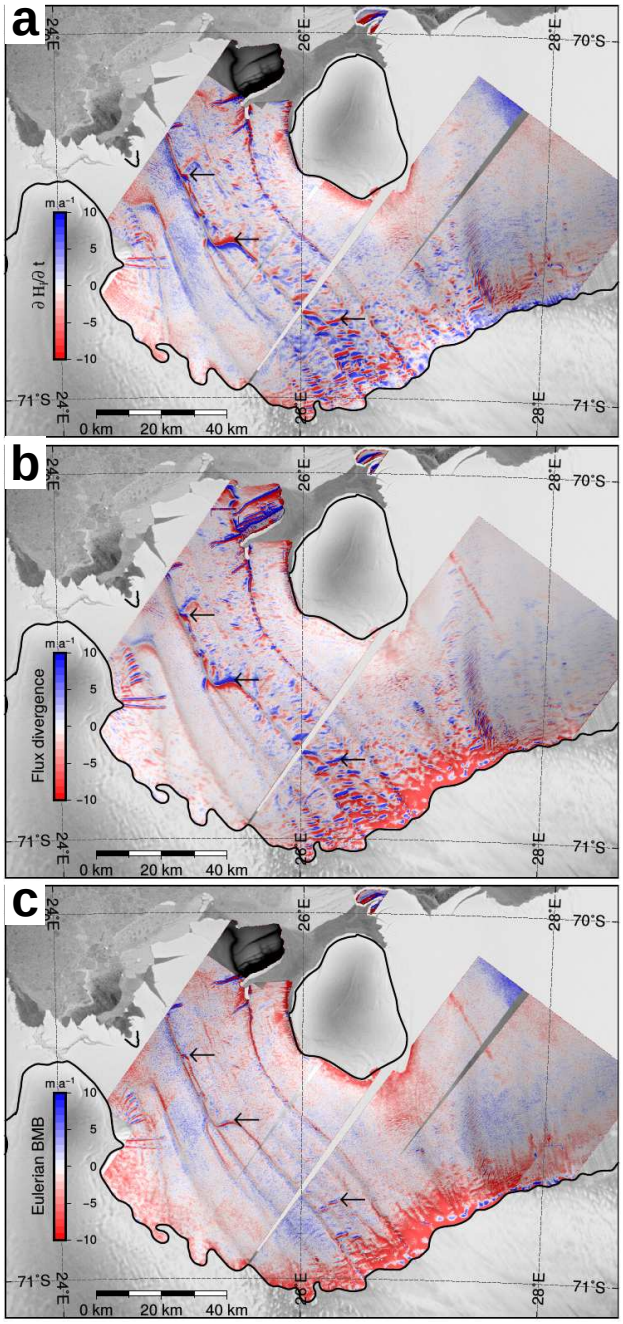

Figure 5. (a) Eulerian thickness change ($\partial H_i/\partial t$) (b) Flux divergence ($\nabla \cdot (H_i \boldsymbol{u})$) and (c) Eulerian basal mass balance (BMB). Arrows point to spurious signal due to advection of ice-shelf channels. The background is from the Radarsat mosaic (Jezek and RAMP-Product-Team, 2002) and the black line delineates the grounding line (Depoorter et al., 2013) .

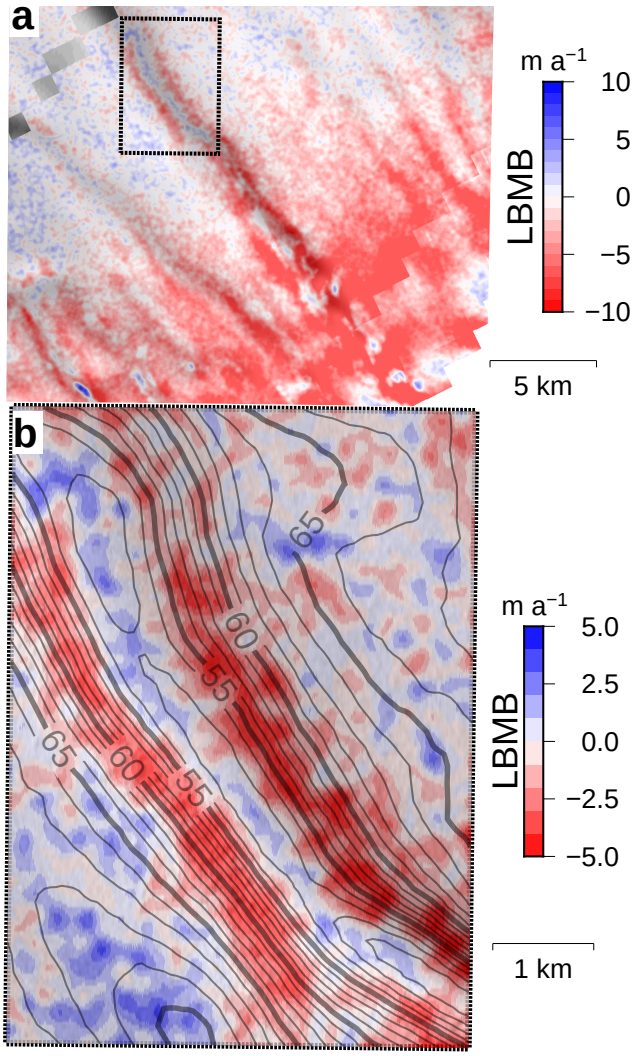

Figure 6. ~~Close-up of the LBMB~~ (a) Ice-shelf channel near the grounding line, where enhanced melting ~~collocates with ice-shelf channels~~ ~~(a) Zoomed-in version of inset a~~ is observed at the channel's flanks. The box is located in Fig. 4. (b) Close-up ~~at one channel~~ view with 1 -m ~~elevation~~ contour lines~~overlain~~.

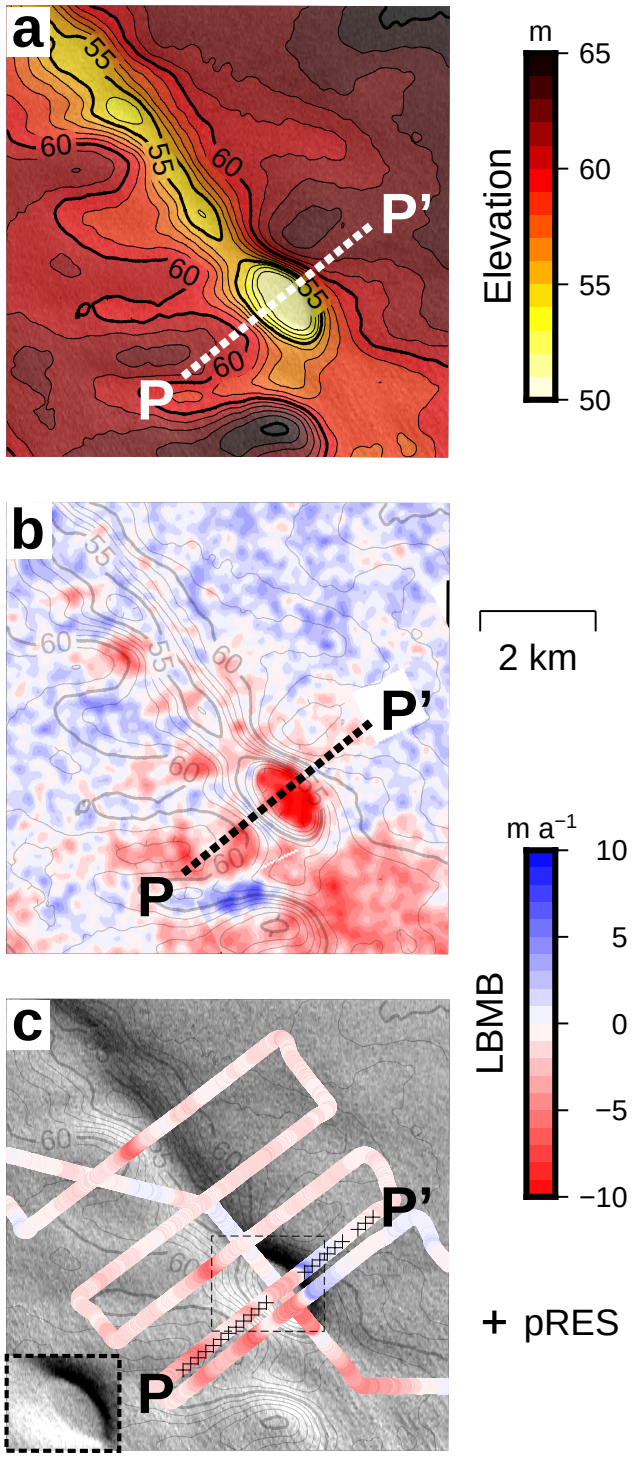

Figure 7. Close-up of the ~~"englacial lake"~~elliptical surface depression, located ~~as inset c~~ in Fig. 4. (a) Surface elevation from ~~the~~ TanDEM-X ~~DEM of~~ DEMs from 2014. (b) LBMB (c) Landsat image of 2014 overlaid with the LBMB computed with elevations from the 2014 TanDEM-X ~~DEM~~ DEMs and the 2016 GNSS profiles (using velocities to shift GNSS elevations backward). The crosses locate phase-sensitive radar (pRES) points. The profile PP' is shown in Fig. 8. ~~Subfigures (a) and (b)~~ All subfigures are overlain with the surface elevation contour lines of 1 m.

ing about -0.5 m a^{-1} with little spatial variability. On the western side – which contains the ~~surface tributaries~~ finger-shaped surface features – larger differences and variability occur. The ~~low~~ differences could reflect the more complex topography and/or temporal variations. The large negative LBMB rates in the ~~englacial lake area are caused by~~ elliptical depression reflect persistent surface lowering of 0.5 to 1.4 m a^{-1}~~because ice-flow~~. Ice-flow divergence is negligible at that location. We extend the time series from the TanDEM-X DEMs to 2016 with the GNSS profiles (Fig. 8c) where we find the same ~~localized~~ localised lowering. This ~~shows~~ indicates that the high-resolution TanDEM-X DEMs reliably pick up surface elevation changes on sub-kilometre scales. Some of the ~~surface tributaries~~ finger-shaped surface depressions also show surface lowering, but less pronounced than what is seen in the ~~englacial lake area~~ elliptical depression itself. The flanks of the ~~ellipsoidal~~ surface depression are significantly steeper on the eastern compared to the western side. Unlike the ~~englacial lake area, the connected~~ elliptical depression, the ice-shelf channel located farther downstream ~~appears inactive. Outside the lake area~~does not actively experience melting or refreezing. Away from ice-shelf channels or other surface depressions, our assumptions for the LBMB (such as hydrostatic equilibrium) likely hold explaining the comparatively good fit with the phase-sensitive radar measurements. Inside the ~~lake area~~elliptical depression, the observed surface lowering ~~must not solely~~ cannot unambigously be attributed to basal melting~~, but may also reflect viscous inflow (Humbert et al., 2015) or creeping of the englacial lake through the ice column~~. Regardless of the specific mechanisms causing the surface lowering, this example highlights that much of the small-scale variability seen in the resulting LBMB field can be used to investigate sub-kilometre-scale ice-shelf processes that do not necessarily occur at the ice-shelf base.

4 Error sources ~~when deriving~~ for the ~~LBMB~~Lagrangian Basal Mass Balance

4.1 Hydrostatic thickness and Lagrangian thickness change

The Lagrangian thickness change is the dominant error source of the LBMB for the Roi Baudouin Ice Shelf, since the magnitude of both ice-flow divergence and SMB ~~for the Roi Baudouin Ice Shelf~~ are one order of magnitude smaller (Fig. 2). The Lagrangian ~~thinning or thickening~~ thickness change depends (i) on factors controlling the hydrostatic ice thickness, i.e. the surface elevation ~~and firn density that define the hydrostatic ice thickness,~~ (above sea level), the seawater and ice densities, the depth of the firnpack and temporal variations thereof; and (ii) on the Lagrangian matching of the DEMs ~~in a Lagrangian framework~~following the ice flow. It should also be clear that our approach is only able to detect basal changes reflected in the surface elevations, because ice thickness is derived from hydrostatic equilibrium.

Calibration and accuracy of TanDEM-X elevations

The interferometric DEMs provide excellent spatial resolution at the cost that they require calibration. It is straightforward to offset the DEMs to account for the relative phase unwrapping using Antarctic-wide DEMs based on altimetry. More challenging are residual phase trends that may originate from imprecise satellite orbits/SAR processing (Drews et al., 2009) or represent unaccounted tilting of the ice-shelf surface due to tides. In our case, these trends are near-linear and become evident in the

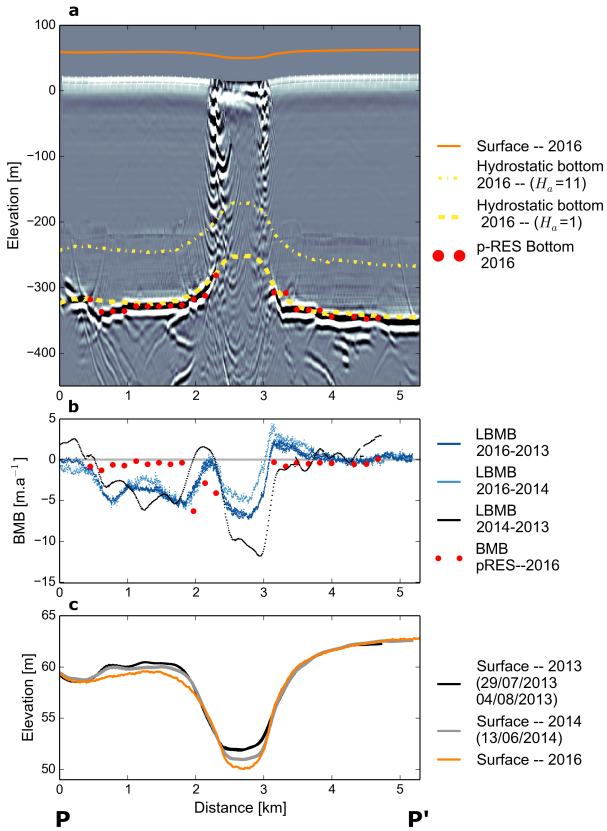

Figure 8. Profile PP' across the ~~ellipsoidal~~ elliptical surface depression located in Fig. 7. (a) ~~Radargram and GNSS surface elevation (Top - GNSS16)~~ Ice thickness from ~~2016~~ profiling and phase-sensitive radars together with the ~~hydrostatic basal elevation (using firn-air content values of 11 and 1) (Bottom - GNSS16) and basal elevation~~ hydrostatically inverted surfaces from ~~phase-sensitive radar (pRES)~~2016, measured with GNSS. (b) ~~LBMB based on phase-sensitive radar measurement in 2016 (pRES16), TanDEM-X elevation changes between~~ Different time slices of the basal mass balance. Data from 2013 and 2014 ~~(TDX13+TDX14) and elevation changes between GNSS and~~ are based on the TanDEM-X ~~profiles (GNSS16+TDX13~~DEMs, ~~GNSS16+TDX14)~~data from 2016 use GNSS surface elevations. (c) Surface lowering at the ~~englacial lake~~elliptical depression: surface elevation between the 2016 GNSS profile ~~of 2016 (GNSS16)~~ and the TanDEM-X profiles from 2013 and ~~2014 (TDX13 and TDX14).~~ 2014. Elevations are referenced to the WGS84 ellipsoid and all profiles are shown in ~~the 2016 geometry.~~Lagrangian coordinates

difference fields of ~~neighbouring DEMs . They systematically~~ overlapping DEMs from both different years and from the exact same date and satellite path. In the former, systematic biases extend in the azimuth direction with residual height differences typically ranging from -0.5 to +0.5 m. Such biases strongly imprint the corresponding LBMB fields resulting in a mosaic with ~~a linear trend~~ linear trends typically ranging from -10 to +10 m a^{-1} in the azimuth direction and ~~cutting edges reaching up to~~ differences exceeding 13 m a^{-1} across seams. To account for this, we ~~applied plane-fitting to~~ correct the 2014 DEMs ~~(section~~ with plane fitting (Sect. 2.4). ~~The adjusted DEMs differ from the~~

We do not correct for systematic trends in individual TanDEM-X frames from the same dates (Fig. S3), not only because the discrepancies are smaller, but also because the small overlapping areas would amplify plane-fitting errors dozens of kilometres away. The standard deviation of the difference fields reduces to 0.3 m after plane fitting. An exception is the two northernmost difference fields, where a trend ranging from -0.8 to 0.8 m remains. In addition to residual phase trends, discrepancies of ~0.5 m can occur in areas where surface slope is locally elevated (e.g ice-shelf channels or surface ridges). Altogether, we therefore estimate the SAR processing uncertainties to be in the order of 0.5 m.

Next, we compare the 2013 and 2014 DEMs with kinematic GNSS profiles ~~collected in 2016 with -0.2~~ from 2012 and 2014, respectively. The time lag between the satellite data acquisition and the collection of ground-truth data is hereby 8-10 months for the 2013 DEMs, and 5-6 months for the 2014 DEMs. For 2012-2013, differences are -0.44±~~1.1~~1.05 m, and for 2014 -0.04±0.65 m. The largest discrepancies occur in both datasets near ice-shelf channels were ice advection within the multiple months time lag is significant (Figs 9). Removing those areas reduces the discrepancies to -0.37±0.29 m in 2012-2013, and -0.07±0.2 m in ~~mean and standard deviation, respectively~~2014. Ignoring the dynamic influence of ice-shelf channels, the highest discrepancies are found in the most upstream part of the 2014 GNSS profile (Fig. 9d). There, TanDEM-X elevations are systematically overestimated by up to 2 m near the grounding line. We attribute this bias to decreasing penetration of the TanDEM-X signal, as the firn-air content decreases towards the grounding zone (Fig. 2a). The X-band radar signal can penetrate up to 8-10 m in cold dry snow (**?**) , and the bulk part of such a signal penetration would be accounted for during our offset correction. However, errors due to spatial variations of signal penetration remain but affect both the 2013 and 2014 DEMs. To conclude, we estimate that in most areas the relative accuracy of the TanDEM-X DEMs is in the sub-meter range. Errors are slightly elevated in areas where the local surface slope is high, and surface elevation is systematically and significantly overestimated by up to 2 m in a narrow belt close to the grounding line.

~~Other uncertainties are rooted in referencing the ellipsoidal~~

Hydrostatic inversion

The main uncertainties for the hydrostatic inversion are referencing the surface elevation to height above sea level~~(using the geoidand~~ , and accounting for density variations. The former depends on the geoid, the mean dynamic topography~~) which we estimate with~~ , tides, atmospheric pressure variations and eustatic sea level. Drews (2015) estimates errors in the geoid and the dynamic topography for RBIS to be within ±1 m~~with little spatial dependency (cf. Drews (2015) for a more detailed discussion on these quantities in the RBIS area)~~. We account for tides and atmospheric pressure variations implicitly by offsetting the

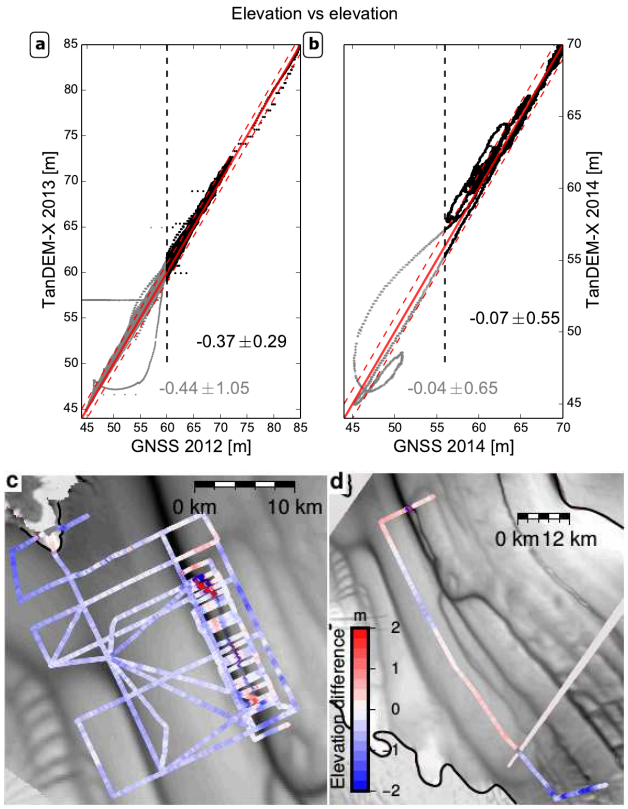

Figure 9. (a – b) Comparison between GNSS 2012 – TandDEM-X 2013 and GNSS 2014 – TanDEM-X 2014, respectively. The GNSS data are located in Fig. 1 with grey points (lying in ice-shelf channels) shown in light blue and light red in the profiles. (c – d) spatial variations of elevation differences between GNSS 2012 – TandDEM-X 2013 and GNSS 2014 – TanDEM-X 2014, respectively. Background is from TanDEM-X elevations.

TanDEM-X DEMs to the CryoSat-2 DEM, which contains these corrections. The smallest component in the error budget are changes in eustatic sea level rise, which we neglect.

~~Along the profile PP',~~ Variations in firn-air content are important because these propagate with a factor of 9 into the hydrostatically inverted ice thickness (Eq. 2). We illustrate this point along profile PP' where the inferred thickness from radar profiling and from phase-sensitive radar agree closely, but the hydrostatic thickness is >80 m thinner (Fig. 8a). Because surface elevation is well constrained by our kinematic GNSS profiles (Fig. 8c), we attribute this large, unphysical mismatch to an overestimation of the firn-air content. The firn densification model predicts a value of 11 m at that location. However, in the field it became evident that this area is close to a spatially extensive blue-ice area where firn-air content is negligible. Reducing the firn-air content to 1 m reconciles the hydrostatic ice thickness with the observed radar ice thickness (Fig. 8a). Such a large deviation of the modelled firn-air content may be site-specific because it is located in the transition zone where turbulent mixing by the katabatic winds and a wind-albedo feedback form a micro-climate that causes extensive surface melting with not

yet fully understood effects on the firn densification (Lenaerts et al., 2017). The impact of the firn-air-content misestimation on the derivation of the hydrostatic ice thickness is further discussed in Lenaerts et al. (2017) . Moreover, Drews et al. (2016) used wide-angle radar measurements in conjunction with ice coring ~~farther seawards and also~~ and found that firn density ~~may vary on small spatial~~ varies spatially over tens of kilometres scales, in particular across ice-shelf channels, where surface melt water collects in the corresponding surface depressions and locally refreezes. Therefore, we anticipate that at least some of the variability seen in the LBMB field is due to unresolved variations in firn density. ~~Fortunately, for the Roi Baudouin Ice Shelf this effect~~

Because of unaccounted variations in firn density, and uncertainties in referencing the freeboard height, our ice thickness field has a lower bound error of at least ±25 m (Drews, 2015) . In some areas the error can be considerably larger. However, the corresponding impact on the inferred LBMB rates is mitigated by the low ice-flow divergence ~~, which renders the absolute value of the hydrostatic~~ rendering the magnitude of ice thickness less important (~~eq. (1~~Eq. (1c)). ~~This may be different for other ice shelves.~~

~~To get our LBMB in a Lagrangian geometry, we matched~~

Lagrangian matching

Computing the Lagrangian thickness change, requires matching the DEMs to account for ice advection. We use a normalised cross-correlation to match 5×5 km ^{2} ~~patches of the two DEMs~~ patches from 2013 ~~and~~ to the 2014 ~~using a cross-correlation algorithm (section 2.1). This method works better than matching the DEMs based on flow vectors (as in Moholdt et al., 2014)~~ geometry (Sect. 2.5). Alternatively, the matching can be based on the surface flow field (Moholdt et al., 2014) . For the DEMs, this methods yields similar results in terms of the large-scale LBMB pattern, but introduces erroneous positive/negative patterns near ice-shelf channels. This is because the ~~interferometrically-derived velocities used here (Fig. 2c) compare well in magnitude with GNSS measurements (Berger et al., 2016) , they are however~~ flow velocities are not sufficiently constrained for the flow direction~~. Tilts~~ , and tilts by a few degrees cause ~~misalignment of ice-shelf channels resulting in an erroneous bimodal pattern in the respective LBMB field. The large-scale LBMB patterns, resulting from the two matching techniques, agree well.~~

a significant mismatch in areas where thickness gradients are larger. On the other hand, the 2016 GNSS have to be matched with the velocities, because 2D cross-correlation fails with profiles.

4.2 Ice-flow divergence: the benefits of regularized derivatives

The high-resolution velocity field is too noisy in magnitude to approximate the derivatives in the flow divergence with finite differencing of neighbouring cells (gridded to 125 m posting). This can be accounted for by smoothing the velocity field ~~, however, we found that this smears out lateral flow convergence near~~ prior to taking the derivative. However, this type of smoothing can blur abrupt changes in the flow velocities and corresponding strain rates. This is important, because we suspect that ice-flow velocities change abruptly in ice-shelf channels ~~(arrows in Fig. 2d). Because enhanced basal melting beneath ice-shelf channels can cause lateral convergence (Drews, 2015) , it is important to preserve this pattern. Wefound that applying the~~ that experience strong basal melting (Drews, 2015) . We, therefore, explore the use of total-variation regularization

~~(Chartrand, 2011) results in the best trade-off between meaningful derivatives and loss of spatial resolution. Fig.~~ which treats abrupt (and discontinuous) changes more accurately (Chartrand, 2011) . Figure 3 illustrates a close-up of an ice-shelf channel (inset ~~b~~ "Fig.3" in Fig. 4) where we compare the ~~velocity divergence and the LBMB based on a smoothed velocity field (averaged within 5.125~~"Normal" (unsmoothed) velocity divergence (b) with its regularized (c) and smoothed (c-e) versions. For the latter, we applied average filters of 375×375 m, 1,125×~~5.125 km^2 moving windows) with the velocity divergence and the LBMB calculated using the total-variation regularization (section 2.6).~~ 1,125 m and 1,875×1,875 m (i.e. kernels of 3×3, 9×9 and 15×15 pixels, respectively) to the velocity field, before computing the gradients. The enhanced velocity-divergence has a similar magnitude in the regularized and the smoothed version using a 375×375 m window. However, the latter is noisier outside the ice-shelf channel than the regularized version. In the regularized case, ~~ice converges more clearly in the channels (velocity divergence up to 3 times lower), which translates in higher basal melt rates (with LBMB 4 m a^{-1}, i.e.~~ velocity divergence at the channel's apex is 8%, ~~~20~~024% ~~, lower) than in the smoothed case. This effect is localised and subtle on the RBIS (because the Lagrangian thickness change primarily controls the LBMB)~~and 40% lower than for the 375×375 m, 1,125×1,125 m and 1,875×1,875 m kernels, respectively. However, the inferred LBMB rates are insensitive to the technical implementation of the derivatives, because the Lagrangrian thickness change controls the signal at RBIS. Nevertheless, ~~this might not be the case~~ in order to study the dynamics of the smaller-scale ice-shelf channels, efficiently denoising the derivatives becomes increasingly important, in particular for ice shelves where ~~dynamic thinning is much stronger. This example shows that a high-resolution BMB field does not only depend on high-resolution thickness fields but also on sufficiently fine velocities and de-noised velocity gradients.~~

~~Close-up of inset b in Fig 4. Comparison of regularized (left: a,c) and smoothed (right: b,d) velocity gradients ($\nabla \cdot \boldsymbol{u}$) and their impact resulting velocity divergence (top: a,b) and LBMB (bottom: c,d). The background image is from Landsat 8, acquired in 2014.~~ the dynamic thinning terms is more important.

4.3 Surface mass balance

Both the firn-air content and the SMB are spatially less well resolved than our ice thickness and velocity fields. Consequently, we do not capture ~~SMB variations~~ their spatial (and temporal) variations on the length scales associated with ice-shelf channels. Both Drews et al. (2016) and Langley et al. (2014) found evidence in the shallow radar stratigraphy that the SMB may be locally elevated in those areas, potentially reflecting the deposition of drifting snow ~~. Those variations, however, occur over a lateral distance of only a few kilometres and are not resolved by the atmospheric model applied here. The subsequent~~ at the bottom of surface slopes (Frezzotti et al., 2007) . If this holds true, then the systematic underestimation of the SMB ~~in the channels therefore results~~ would result in a positive bias of the LBMB in ~~these~~ those areas.

5 Spatial variability of the Lagrangian basal mass balance

The large-scale patches of enhanced basal melting (~~section 3; labels 1-3~~ Sect. 3.1; labels A-C in Fig. 4) are sufficiently far away from the tidal bending zone so that we can safely assume hydrostatic equilibrium. ~~This means that the LBMB likely reflects~~

~~the true BMB at the ice-shelf base. These regions (especially patches 1 and 2)~~ These regions are also detected by Rignot et al. (2013), based on different input datasets ~~, and~~ (i.e. Eulerian thickness change based on ICESat-1). Patches A-C line up with deepest parts of the ice-shelf base and the largest gradients in the hydrostatic ice thickness~~, suggesting that the enhanced basal melting is driven by the basal ice-shelf slope. Those steeper parts facilitate the slope-dependent~~ . A large ice draft fosters basal melting because the freezing point is lower with depth (e.g. Holland et al., 2008) . The steep basal slopes facilitate entrainment of heat in the mixed layer beneath the ice shelf increasing basal melting (Jenkins and Doake, 1991; Little et al., 2009).

~~As we have seen, some of the observed variability may reflect unresolved spatial variability~~ The smaller-scale variations in LBMB are more difficult to interpret, because these are overlain by unaccounted variations in firn density~~(Drews et al., 2016) or surface lowering~~ , SMB, and ice that is not ~~hydrostatically compensated. Interpreting the LBMB on sub-kilometre scales is therefore not straightforward. However~~in hydrostatic equilibrium. Nevertheless, the comparison with the phase-sensitive radar data and the kinematic GNSS profiling increases our confidence that much of the relative variability that we observe here is ~~not due to noise. This is most clearly shown for the englacial lake area where the localised surface lowering is consistently observed in different datasets~~ meaningful. The surface lowering of the elliptical surface depression is consistently shown over a 3-year time period ~~. This makes this region dynamically active, although the signal does not necessarily indicate localised basal melting~~marking this zone as dynamically active. Two other options are: (i) a transient adjustment of the surface towards hydrostatic equilibrium (Humbert et al., 2015) as a response to some unknown event in the past which locally reduced the ice thickness, and (ii) the surface lowering may reflect vertical creeping of a liquid water body through the ice column. In any case, the surface lowering is restricted to a small area and the ice-shelf channel farther downstream appears passive (i.e. does not show significant melting nor refreezing).

In most areas, ice-shelf channels at RBIS seem to advect passively and basal melt rates there do not significantly stand out from those in the larger surrounding. ~~We find however some evidence for~~ Exceptions are the locally elevated basal melt rates in ice-shelf channels in the ~~ice-shelf's interior~~ interior of the RBIS (e.g. inset ~~b in Fig. 4,~~ "Fig. 3" in Fig. ~~3c~~4) and close to the grounding zone (~~inset a~~ Fig.6 and its corresponding inset in Fig. 4~~, Fig.6~~). Almost all ice-shelf channels at RBIS are connected to the grounding line and may ~~originate~~ arise from water-filled subglacial conduits injecting ~~basal-melt~~ sublglacial-melt water into the ice-shelf cavity, driving a spatially localised buoyant melt-water plume ~~(Jenkins, 2011; Le Brocq et al., 2013)~~ (Jenkins, 2011; Le Br
Such localised melting near the grounding zone has been previously observed on Pine Island Ice Shelf using similar methods as done here (Dutrieux et al., 2013). However, on Pine Island Ice Shelf, background melt rates are an order of magnitude larger than what is observed here (Depoorter et al., 2013; Rignot et al., 2013) and Dutrieux et al. (2013) analysed DEMs separated by 3 years (compared to the 1 year time period used here). This explains why ~~the BMB gradients~~ locally elevated BMB values appear more clearly ~~in those cases. In areas where the LBMB is elevated beneath ice-shelf channels, we~~ on other ice shelves. We find some evidence that basal melting is concentrated on the flanks, rather than on the apex (Fig. 6). This accords both with observations (Dutrieux et al., 2014) and modelling (Millgate et al., 2013). ~~Inside the channels, those studies show strongest (weakest) melting on the flank (at the apex) of the channels and moderate melting between them. Dutrieux et al. (2014) explain this pattern with~~ Dutrieux et al. (2014) suggest that the presence of a colder water ~~layer (formed by mixing of melt and sea water (Rignot and Steffen, 2008)) that~~ blocks the heat flux from below near the apex of the channel. Alternatively, modelling

~~(Millgate et al., 2013) suggests~~ suggests (Millgate et al., 2013) that a geostrophic current develops beneath the channels (if the channels are wide enough) which preferentially melts at the channel's flanks. This seems less likely here because ice-shelf channels near the grounding line are narrow (i.e. a few hundred meters wide and high).

In summary, our ~~combination of satellite observations with field data shows that much of the sub-kilometric variability that we observe in the LBMB field is above the signal-to-noise ratio. This highlights that ice-ocean interactions vary spatially over the entire ice shelf and implies that~~ observations suggest that the LBMB varies on multiple spatial scales which has several implications. First, point measurements with phase-sensitive radars are not necessarily representative for a larger area. ~~Instead~~Particularly in areas where thickness gradients are large, phase-sensitive radar measurements are best understood in combination with satellite-based estimates covering larger spatial scales. On the other hand, on-site point measurements are crucial to estimate the quality of the satellite-based BMB estimates which, are uncertain in their magnitude. Second, this sub-kilometre variability in ice-ocean processes poses challenges for coupling ice with ocean models, because highly resolved oceanic models, typically gridded with 1-2 km (Dinniman et al., 2016) , and community efforts, such as the Marine Ice Sheet–Ocean Model Intercomparison Project (MISOMIP), prescribe horizontal gridding of 2 km (Asay-Davis et al., 2016) . This is too coarse to capture the spatial variability that we observe here.

6 Conclusions

We ~~have~~ derived the Lagrangian Basal Mass Balance (LBMB) of the Roi Baudouin Ice Shelf by combining TanDEM-X DEMs of 2013 and 2014 with high-resolution surface velocities and atmospheric modelling outputs. On a large scale, the LBMB shows the highest basal melt rates where the ice draft is deepest and steepest, i.e. close to the grounding line and near Derwael Ice Rise and the Western Ice Promontory. This pattern is overlain with significant sub-kilometre scale variability, as witnessed by localised surface lowering of ~~a (potentially refrozen) englacial lake~~ an elliptical surface depression and large basal melting rates below ice-shelf channels. For the latter, we find evidence that at least in some areas, basal melting is concentrated on the channel's flanks as opposed to its apex. Key advancements in our methodology to elucidate this variability are (i) the calibration of the DEMs to account for residual trends from the interferometric processing, (ii) the quality of the matching procedure – using normalised cross-correlation coefficients – for calculating the Lagrangian thickness change , and (iii) the total-variation regularization of the spatial derivatives that preserves ~~small-scale flow anomalies near~~ abrupt changes in flow velocities that are sometimes observed across ice-shelf channels. New satellites (such as TanDEM-X or Sentinel 1) will continue to provide highly-resolved datasets of surface elevation and ice velocity. In comparison, atmospheric modelling does not (yet) provide the required spatial resolution on firn-density and SMB to solve the mass budget reliably on sub-kilometre scales. Although the uncertainty of the absolute LBMB values remains high, we find a good fit with on-site measurements from phase-sensitive radar, and we demonstrate that much of the spatial LBMB variability contains information about ice-shelf processes occurring at sub-kilometre scales. This variability highlights the complexity of the ice-ocean and ice-atmosphere interactions on small spatial scales on ice shelves, which need to be accounted for by glaciologists, oceanographers and atmospheric scientists.

Table 1. Input datasets

Type of data	~~Technique used~~	**Observations/Modelling** Reference	Dataset/Model	~~literature~~ gridding	Use (Eq.)
Surface elevation	~~observation~~	**Observations** this study	TanDEM-X	~~this study~~ 10 m	$\frac{\mathrm{D}H}{\mathrm{D}t}$, H $\frac{\mathrm{D}H_i}{\mathrm{D}t}$,
Velocity	~~observation~~	**Observations** Berger et al. (2016)	ERS1/2 ALOS PALSAR	~~Berger et al. (2016)~~ 125 m	$\nabla \cdot \boldsymbol{u}$
Surface Mass Balance	~~modelling~~	**Modelling** Lenaerts et al. (2017, 2014)	RACMO 2.3	~~Lenaerts et al. (2017, 2014)~~ 5.5 km	SMB $\dot{M}_s$
Firn-air content	~~modelling~~	**Modelling** Lenaerts et al. (2017) Ligtenberg et al. (2011)	RACMO 2.3	5.5 km	H H_i
Mean Dynamic topography	~~modelling~~	**Modelling & observations** Knudsen and Andersen (2012)	DTU12MDT	~~Knudsen and Andersen (2012)~~ 0.125°	H H_i
Geoid	~~modelling~~	**Modelling & observations** Förste et al. (2014)	EIGEN-6C4	~~Förste et al. (2014)~~ 0.125°	H H_i

Appendix A: Input data

Table 1 characterises the main input variable in Eq. (1~~).~~ c).

Acknowledgements. This paper forms a contribution to the Belgian Research Programme on the Antarctic (Belgian Federal Science Policy Office), project SD/CA/06A (Constraining Ice Mass Change in Antarctica, IceCon). S. Berger is supported by a FRS-FNRS (Fonds de la Recherche Scientifique) "Aspirant" PhD fellowship. R. Drews was partially supported by the Deutsche Forschungsgemeinschaft (DFG) in the framework of the priority programme "Antarctic Research with comparative investigations in Arctic ice areas" by the grant MA 3347/10-1. S. Sun is supported by the FNRS-PDR (Fonds de la Recherche Scientifique) project MEDRISM. TanDEM-X data originate from German Aerospace Center (ATI-GLAC0267). We thank Nicolas Bergeot (Royal Observatory Belgium) who helped with GNSS processing and K. Nicholls for his valuable help in processing of the phase-sensitive radar. We received excellent logistic support by the Belgian Military, AntarctiQ and the International Polar Foundation during the field campaigns. Finally, we thank J. Lenaerts and S. Ligtenberg for sharing results from atmospheric modelling, as well as D. Shean and G. Moholdt for their constructive comments on this manuscript.

References

Asay-Davis, X. S., Cornford, S. L., Durand, G., Galton-Fenzi, B. K., Gladstone, R. M., Hilmar Gudmundsson, G., Hattermann, T., Holland, D. M., Holland, D., Holland, P. R., Martin, D. F., Mathiot, P., Pattyn, F., and Seroussi, H.: Experimental design for three interrelated marine ice sheet and ocean model intercomparison projects: MISMIP v. 3 (MISMIP +), ISOMIP v. 2 (ISOMIP +) and MISOMIP v. 1 (MISOMIP1), Geoscientific Model Development, 9, 2471–2497, doi:10.5194/gmd-9-2471-2016, http://www.geosci-model-dev.net/9/2471/2016/, 2016.

Banwell, A. F., MacAyeal, D. R., and Sergienko, O. V.: Breakup of the Larsen B Ice Shelf triggered by chain reaction drainage of supraglacial lakes, Geophysical Research Letters, 40, 5872–5876, doi:10.1002/2013GL057694, http://doi.wiley.com/10.1002/2013GL057694, 2013.

Berger, S., Favier, L., Drews, R., Derwael, J. J., and Pattyn, F.: The control of an uncharted pinning point on the flow of an Antarctic ice shelf, Journal of Glaciology, 62, 37–45, doi:10.1017/jog.2016.7, http://journals.cambridge.org/abstract{_}S0022143016000071, 2016.

Berthier, E., Cabot, V., Vincent, C., and Six, D.: Decadal Region-Wide and Glacier-Wide Mass Balances Derived from Multi-Temporal ASTER Satellite Digital Elevation Models. Validation over the Mont-Blanc Area, Frontiers in Earth Science, 4, 63, doi:10.3389/feart.2016.00063, http://journal.frontiersin.org/Article/10.3389/feart.2016.00063/abstract, 2016.

Bindschadler, R., Choi, H., Wichlacz, A., Bingham, R., Bohlander, J., Brunt, K., Corr, H., Drews, R., Fricker, H., Hall, M., Hindmarsh, R., Kohler, J., Padman, L., Rack, W., Rotschky, G., Urbini, S., Vornberger, P., and Young, N.: Getting around Antarctica: New high-resolution mappings of the grounded and freely-floating boundaries of the Antarctic ice sheet created for the International Polar Year, The Cryosphere, 5, 569–588, doi:10.5194/tc-5-569-2011, http://www.the-cryosphere.net/5/569/2011/tc-5-569-2011.html, 2011a.

Bindschadler, R., Vaughan, D. G., and Vornberger, P.: Variability of basal melt beneath the Pine Island Glacier ice shelf, West Antarctica, Journal of Glaciology, 57, 581–595, doi:10.3189/002214311797409802, http://www.ingentaconnect.com/content/igsoc/jog/2011/00000057/00000204/art00001, 2011b.

Bradski, G. and Kaehler, A.: 07 Learning OpenCV: Computer Vision with the OpenCV Library, vol. 1, doi:10.1109/MRA.2009.933612, https://books.google.be/books?hl=en{&}lr={&}id=seAgiOfu2EIC{&}oi=fnd{&}pg=PR3{&}dq=Learning+OpenCV:+Computer+Vision+with+the+OpenCV+Library{&}ots=hTM9cndALg{&}sig=zUae2{_}vroNwcUaLv7SQOfb6MxUohttp://www.amazon.com/dp/0596516134, 2008.

Callens, D., Matsuoka, K., Steinhage, D., Smith, B., Witrant, E., and Pattyn, F.: Transition of flow regime along a marine-terminating outlet glacier in East Antarctica, The Cryosphere, 8, 867–875, doi:10.5194/tc-8-867-2014, http://www.the-cryosphere.net/8/867/2014/tc-8-867-2014.html, 2014.

Callens, D., Drews, R., Witrant, E., Philippe, M., and Pattyn, F.: Temporally stable surface mass balance asymmetry across an Ice rise derived from radar internal reflection horizons through inverse modeling, Journal of Glaciology, 62, 525–534, doi:10.1017/jog.2016.41, http://www.journals.cambridge.org/abstract{_}S0022143016000411, 2016.

Chartrand, R.: Numerical Differentiation of Noisy, Nonsmooth Data, ISRN Applied Mathematics, 2011, 1–11, doi:10.5402/2011/164564, http://downloads.hindawi.com/journals/isrn.applied.mathematics/2011/164564.pdf, 2011.

Church, J. A., White, N. J., Coleman, R., Lambeck, K., and Mitrovica, J. X.: Estimates of the regional distribution of sea level rise over the 1950-2000 period, Journal of Climate, 17, 2609–2625, doi:10.1175/1520-0442(2004)017<2609:EOTRDO>2.0.CO;2, http://journals.ametsoc.org/doi/abs/10.1175/1520-0442{%}282004{%}29017{%}3C2609{%}3AEOTRDO{%}3E2.0.CO{%}3B2, 2004.

Chuter, S. J. and Bamber, J. L.: Antarctic ice shelf thickness from CryoSat-2 radar altimetry, Geophysical Research Letters, 42, 10,710–721,729, doi:10.1002/2015GL066515, http://dx.doi.org/10.1002/2015GL066515, 2015.

DeConto, R. M. and Pollard, D.: Contribution of Antarctica to past and future sea-level rise, Nature, 531, 591–597, doi:10.1038/nature17145, http://dx.doi.org/10.1038/nature17145, 2016.

Dehecq, A., Millan, R., Berthier, E., Gourmelen, N., Trouve, E., and Vionnet, V.: Elevation Changes Inferred From TanDEM-X Data Over the Mont-Blanc Area: Impact of the X-Band Interferometric Bias, IEEE Journal of Selected Topics in Applied Earth Observations and Remote Sensing, 9, 3870–3882, doi:10.1109/JSTARS.2016.2581482, http://ieeexplore.ieee.org/document/7518587/, 2016.

Depoorter, M. A., Bamber, J. L., Griggs, J. a., Lenaerts, J. T. M., Ligtenberg, S. R. M., van den Broeke, M. R., and Moholdt, G.: Calving fluxes and basal melt rates of Antarctic ice shelves., Nature, 502, 89–92, doi:10.1038/nature12567, http://www.ncbi.nlm.nih.gov/pubmed/24037377, 2013.

Dinniman, M., Asay-Davis, X., Galton-Fenzi, B., Holland, P., Jenkins, A., and Timmermann, R.: Modeling Ice Shelf/Ocean Interaction in Antarctica: A Review, Oceanography, 29, 144–153, doi:10.5670/oceanog.2016.106, http://www.tos.org/oceanography/article/modeling-ice-shelf-ocean-interaction-in-antarctica-a-review, 2016.

Drews, R.: Evolution of ice-shelf channels in Antarctic ice shelves, The Cryosphere, 9, 1169–1181, doi:doi:10.5194/tc-9-1169-2015, http://www.the-cryosphere.net/9/1169/2015/tc-9-1169-2015.html, 2015.

Drews, R., Rack, W., Wesche, C., and Helm, V.: A Spatially Adjusted Elevation Model in Dronning Maud Land, Antarctica, Based on Differential SAR Interferometry, IEEE Transactions on Geoscience and Remote Sensing, 47, 2501–2509, doi:10.1109/TGRS.2009.2016081, http://ieeexplore.ieee.org/articleDetails.jsp?arnumber=4895338, 2009.

Drews, R., Matsuoka, K., Martín, C., Callens, D., Bergeot, N., and Pattyn, F.: Evolution of Derwael Ice Rise in Dronning Maud Land, Antarctica, over the last millennia, Journal of Geophysical Research: Earth Surface, 120, 564–579, doi:10.1002/2014JF003246, http://doi.wiley.com/10.1002/2014JF003246, 2015.

Drews, R., Brown, J., Matsuoka, K., Witrant, E., Philippe, M., Hubbard, B., and Pattyn, F.: Constraining variable density of ice shelves using wide-angle radar measurements, The Cryosphere, 10, 811–823, doi:10.5194/tc-10-811-2016, http://www.the-cryosphere.net/10/811/2016/, 2016.

Drews, R., Pattyn, F., Hewitt, I. J., Ng, F. S. L., Berger, S., Matsuoka, K., Helm, V., Bergeot, N., Favier, L., and Neckel, N.: Actively evolving subglacial conduits and eskers initiate ice shelf channels at an Antarctic grounding line, Nature Communications, 8, 15 228, doi:10.1038/ncomms15228, http://www.nature.com/doifinder/10.1038/ncomms15228, 2017.

Dutrieux, P., Vaughan, D. G., Corr, H. F. J., Jenkins, A., Holland, P. R., Joughin, I., and Fleming, A.: Pine Island Glacier ice shelf melt distributed at kilometre scales, The Cryosphere, 7, 1591–1620, 2013.

Dutrieux, P., Stewart, C., Jenkins, A., Nicholls, K. W., Corr, H. F. J., Rignot, E., and Steffen, K.: Basal terraces on melting ice shelves, Geophysical Research Letters, 41, 5506–5513, 2014.

Favier, L., Gagliardini, O., Durand, G., and Zwinger, T.: A three-dimensional full Stokes model of the grounding line dynamics: effect of a pinning point beneath the ice shelf, The Cryosphere, 6, 101–112, doi:10.5194/tc-6-101-2012, http://www.the-cryosphere.net/6/101/2012/tc-6-101-2012.html, 2012.

Favier, L., Durand, G., Cornford, S. L., Gudmundsson, G. H., Gagliardini, O., Gillet-Chaulet, F., Zwinger, T., Payne, A. J., and Le Brocq, A. M.: Retreat of Pine Island Glacier controlled by marine ice-sheet instability, Nature Climate Change, 4, 117–121, doi:10.1038/nclimate2094, http://dx.doi.org/10.1038/nclimate2094, 2014.

Favier, L., Pattyn, F., Berger, S., and Drews, R.: Dynamic influence of pinning points on marine ice-sheet stability: a numerical study in Dronning Maud Land, East Antarctica, The Cryosphere, 10, 2623–2635, doi:10.5194/tc-10-2623-2016, http://www.the-cryosphere.net/10/2623/2016/, 2016.

Förste, C., Bruinsma, S., Abrikosov, O., Flechtner, F., Marty, J.-C., Lemoine, J.-M., Dahle, C., Neumayer, H., Barthelmes, F., König, R., and Biancale, R.: EIGEN-6C4 - The latest combined global gravity field model including GOCE data up to degree and order 1949 of GFZ Potsdam and GRGS Toulouse, in: EGU General Assembly Conference Abstracts, vol. 16 of *EGU General Assembly Conference Abstracts*, p. 3707, 2014.

Frezzotti, M., Urbini, S., Proposito, M., Scarchilli, C., and Gandolfi, S.: Spatial and temporal variability of surface mass balance near Talos Dome, East Antarctica, Journal of Geophysical Research, 112, F02 032, doi:10.1029/2006JF000638, http://doi.wiley.com/10.1029/2006JF000638, 2007.

Gladish, C. V., Holland, D. M., Holland, P. R., and Price, S. F.: Ice-shelf basal channels in a coupled ice/ocean model, Journal of Glaciology, 58, 1227–1244, doi:10.3189/2012JoG12J003, 2012.

Golledge, N. R., Menviel, L., Carter, L., Fogwill, C. J., England, M. H., Cortese, G., and Levy, R. H.: Antarctic contribution to meltwater pulse 1A from reduced Southern Ocean overturning, Nature Communications, 5, 1–10, doi:10.1038/ncomms6107, http://www.nature.com/doifinder/10.1038/ncomms6107, 2014.

Golledge, N. R., Kowalewski, D. E., Naish, T. R., Levy, R. H., Fogwill, C. J., and Gasson, E. G. W.: The multi-millennial Antarctic commitment to future sea-level rise, Nature, 526, 421–425, doi:10.1038/nature15706, http://www.nature.com/doifinder/10.1038/nature15706, 2015.

Gudmundsson, G. H., Krug, J., Durand, G., Favier, L., and Gagliardini, O.: The stability of grounding lines on retrograde slopes, The Cryosphere, 6, 1497–1505, doi:10.5194/tc-6-1497-2012, http://www.the-cryosphere.net/6/1497/2012/, 2012.

Helm, V., Humbert, A., and Miller, H.: Elevation and elevation change of Greenland and Antarctica derived from CryoSat-2, The Cryosphere, 8, 1539–1559, doi:10.5194/tc-8-1539-2014, http://www.the-cryosphere.net/8/1539/2014/, 2014.

Holland, P. R., Jenkins, A., and Holland, D. M.: The Response of Ice Shelf Basal Melting to Variations in Ocean Temperature, Journal of Climate, 21, 2558–2572, doi:10.1175/2007JCLI1909.1, http://journals.ametsoc.org/doi/abs/10.1175/2007JCLI1909.1, 2008.

Hulbe, C. L., MacAyeal, D. R., Denton, G. H., Kleman, J., and Lowell, T. V.: Catastrophic ice shelf breakup as the source of Heinrich event icebergs, Paleoceanography, 19, n/a–n/a, doi:10.1029/2003PA000890, http://doi.wiley.com/10.1029/2003PA000890, 2004.

Humbert, A., Steinhage, D., Helm, V., Hoerz, S., Berendt, J., Leipprand, E., Christmann, J., Plate, C., and Müller, R.: On the link between surface and basal structures of the Jelbart Ice Shelf, Antarctica, Journal of Glaciology, 61, 975–986, doi:10.3189/2015JoG15J023, http://www.ingentaconnect.com/content/igsoc/jog/2015/00000061/00000229/art00013, 2015.

Jenkins, A.: Convection-driven melting near the grounding lines of ice shelves and tidewater glaciers, Journal of Physical Oceanography, 41, 2279–2294, 2011.

Jenkins, A. and Doake, C. S. M.: Ice-ocean interaction on Ronne Ice Shelf, Antarctica, Journal of Geophysical Research, 96, 791, doi:10.1029/90JC01952, http://doi.wiley.com/10.1029/90JC01952, 1991.

Jezek, K. and RAMP-Product-Team: RAMP AMM-1 SAR Image Mosaic of Antarctica, Fairbanks, AK: Alaska Satellite Facility, in association with the National Snow and Ice Data Center, Boulder, CO. Digital media, 2002.

Joughin, I.: Ice-sheet velocity mapping: a combined interferometric and speckle-tracking approach, Annals of Glaciology, 34, 195–201, 2002.

Knudsen, P. and Andersen, O. B.: A global mean ocean circulation estimation using goce gravity models - the DTU12MDT mean dynamic topography model, in: 20 Years of Progress in Radar Altimetry Symposium, p. 123, 2012.

Krieger, G., Moreira, A., Fiedler, H., Hajnsek, I., Werner, M., Younis, M., and Zink, M.: TanDEM-X: A Satellite Formation for High-Resolution SAR Interferometry, IEEE Transactions on Geoscience and Remote Sensing, 45, 3317–3341, doi:10.1109/TGRS.2007.900693, http://ieeexplore.ieee.org/lpdocs/epic03/wrapper.htm?arnumber=4373373, 2007.

Langley, K., Deschwanden, A., Kohler, J., Sinisalo, A., Matsuoka, K., Hattermann, T., Humbert, A., Nøst, O. A., and Isaksson, E.: Complex network of channels beneath an Antarctic ice shelf, Geophysical Research Letters, 41, 1209–1215, 2014.

Le Brocq, A. M., Ross, N., Griggs, J. A., Bingham, R. G., Corr, H. F. J., Ferraccioli, F., Jenkins, A., Jordan, T. A., Payne, A. J., Rippin, D. M., and Others: Evidence from ice shelves for channelized meltwater flow beneath the Antarctic Ice Sheet, Nature Geoscience, 6, 945–948, 2013.

Lenaerts, J., Brown, J., Van Den Broeke, M. R., Matsuoka, K., Drews, R., , Callens, D., Philippe, M., Gorodetskaya, I. V., Van Meijgaard, E., Reijmer, C. H., and Others: High variability of climate and surface mass balance induced by Antarctic ice rises, Journal of Glaciology, 60, 1101, http://www.staff.science.uu.nl/{~}lenae101/pubs/Lenaerts2014c.pdf, 2014.

Lenaerts, J. T. M., Lhermitte, S., Drews, R., Ligtenberg, S. R. M., Berger, S., Helm, V., Smeets, C. J. P. P., van den Broeke, M. R., van de Berg, W. J., van Meijgaard, E., Eijkelboom, M., Eisen, O., and Pattyn, F.: Meltwater produced by wind–albedo interaction stored in an East Antarctic ice shelf, Nature Climate Change, 7, 58–62, doi:10.1038/nclimate3180, http://www.nature.com/doifinder/10.1038/nclimate3180{%}5Cnhttp://www.benemelt.eu/benemelt{#}74887, 2017.

Ligtenberg, S. R. M., Helsen, M. M., and van den Broeke, M. R.: An improved semi-empirical model for the densification of Antarctic firn, The Cryosphere, 5, 809–819, doi:10.5194/tc-5-809-2011, http://www.the-cryosphere.net/5/809/2011/tc-5-809-2011.html, 2011.

Little, C. M., Gnanadesikan, A., and Oppenheimer, M.: How ice shelf morphology controls basal melting, Journal of Geophysical Research, 114, C12 007, doi:10.1029/2008JC005197, http://doi.wiley.com/10.1029/2008JC005197, 2009.

Marengoni, M. and Stringhini, D.: High Level Computer Vision Using OpenCV, in: 2011 24th SIBGRAPI Conference on Graphics, Patterns, and Images Tutorials, pp. 11–24, IEEE, doi:10.1109/SIBGRAPI-T.2011.11, http://ieeexplore.ieee.org/document/6076745/, 2011.

Marsh, O. J., Fricker, H. A., Siegfried, M. R., Christianson, K., Nicholls, K. W., Corr, H. F. J., and Catania, G.: High basal melting forming a channel at the grounding line of Ross Ice Shelf, Antarctica, Geophysical Research Letters, pp. n/a–n/a, doi:10.1002/2015GL066612, http://doi.wiley.com/10.1002/2015GL066612, 2016.

Matsuoka, K., Pattyn, F., Callens, D., and Conway, H.: Radar characterization of the basal interface across the grounding zone of an ice-rise promontory in East Antarctica, Annals of Glaciology, 53, 29–34, doi:10.3189/2012AoG60A106, http://www.ingentaconnect.com/content/igsoc/agl/2012/00000053/00000060/art00004, 2012.

Mercer, J. H.: West Antarctic ice sheet and CO2 greenhouse effect: a threat of disaster, Nature, 271, 321–325, doi:10.1038/271321a0, http://www.nature.com/doifinder/10.1038/271321a0, 1978.

Millgate, T., Holland, P. R., Jenkins, A., and Johnson, H. L.: The effect of basal channels on oceanic ice-shelf melting, Journal of Geophysical Research: Oceans, 118, 6951–6964, doi:10.1002/2013JC009402, http://dx.doi.org/10.1002/2013JC009402, 2013.

Moholdt, G., Padman, L., and Fricker, H. A.: Basal mass budget of Ross and Filchner-Ronne ice shelves, Antarctica, derived from Lagrangian analysis of ICESat altimetry, Journal of Geophysical Research: Earth Surface, 2014.

Neckel, N., Drews, R., Rack, W., and Steinhage, D.: Basal melting at the Ekström Ice Shelf, Antarctica, estimated from mass flux divergence, Annals of Glaciology, 53, 294–302, doi:10.3189/2012AoG60A167, http://www.ingentaconnect.com/content/igsoc/agl/2012/00000053/00000060/art00035, 2012.

Nicholls, K. W., Corr, H. F., Stewart, C. L., Lok, L. B., Brennan, P. V., and Vaughan, D. G.: A ground-based radar for measuring vertical strain rates and time-varying basal melt rates in ice sheets and shelves, Journal of Glaciology, 61, 1079–1087, doi:10.3189/2015JoG15J073, http://www.ingentaconnect.com/content/igsoc/jog/2015/00000061/00000230/art00005, 2015.

Padman, L., Fricker, H. A., Coleman, R., Howard, S., and Erofeeva, L.: A new tide model for the Antarctic ice shelves and seas, Annals of Glaciology, 34, 247–254, 2002.

Padman, L., Erofeeva, S. Y., and Fricker, H. A.: Improving Antarctic tide models by assimilation of ICESat laser altimetry over ice shelves, Geophysical Research Letters, 35, L22 504, doi:10.1029/2008GL035592, http://doi.wiley.com/10.1029/2008GL035592, 2008.

Paolo, F. S., Fricker, H. A., and Padman, L.: Volume loss from Antarctic ice shelves is accelerating., Science, 348, 327–331, doi:10.1126/science.aaa0940, http://www.sciencemag.org/content/348/6232/327.fullhttp://www.sciencemag.org/content/early/2015/03/31/science.aaa0940.abstract, 2015.

Pattyn, F., Perichon, L., Durand, G., Favier, L., Gagliardini, O., Hindmarsh, R. C., Zwinger, T., Albrecht, T., Cornford, S., Docquier, D., Fürst, J. J., Goldberg, D., Gudmundsson, G. H., Humbert, A., Hütten, M., Huybrechts, P., Jouvet, G., Kleiner, T., Larour, E., Martin, D., Morlighem, M., Payne, A. J., Pollard, D., Rückamp, M., Rybak, O., Seroussi, H., Thoma, M., and Wilkens, N.: Grounding-line migration in plan-view marine ice-sheet models: results of the ice2sea MISMIP3d intercomparison, Journal of Glaciology, 59, 410–422, doi:10.3189/2013JoG12J129, http://www.ingentaconnect.com/content/igsoc/jog/2013/00000059/00000215/art00002, 2013.

Pritchard, H. D., Ligtenberg, S. R. M., Fricker, H. A., Vaughan, D. G., van den Broeke, M. R., and Padman, L.: Antarctic ice-sheet loss driven by basal melting of ice shelves., Nature, 484, 502–5, doi:10.1038/nature10968, http://dx.doi.org/10.1038/nature10968, 2012.

Rignot, E. and Steffen, K.: Channelized bottom melting and stability of floating ice shelves, Geophysical Research Letters, 35, 2008.

Rignot, E., Mouginot, J., and Scheuchl, B.: Antarctic grounding line mapping from differential satellite radar interferometry, Geophysical Research Letters, 38, doi:10.1029/2011GL047109, 2011a.

Rignot, E., Mouginot, J., and Scheuchl, B.: Ice flow of the Antarctic ice sheet, Science, 333, 1427–1430, doi:10.1126/science.1208336, 2011b.

Rignot, E., Jacobs, S., Mouginot, J., and Scheuchl, B.: Ice-shelf melting around Antarctica, Science, 341, 266–270, doi:10.1126/science.1235798, 2013.

Rignot, E., Mouginot, J., Morlighem, M., Seroussi, H., and Scheuchl, B.: Widespread, rapid grounding line retreat of Pine Island, Thwaites, Smith, and Kohler glaciers, West Antarctica, from 1992 to 2011, Geophysical Research Letters, 2014.

Ritz, C., Edwards, T. L., Durand, G., Payne, A. J., Peyaud, V., and Hindmarsh, R. C. A.: Potential sea-level rise from Antarctic ice-sheet instability constrained by observations, Nature, 528, 115–118, doi:10.1038/nature16147, http://dx.doi.org/10.1038/nature16147, 2015.

Scambos, T. A., Bohlander, J. A., Shuman, C. A., and Skvarca, P.: Glacier acceleration and thinning after ice shelf collapse in the Larsen B embayment, Antarctica, Geophysical Research Letters, 31, L18 402, doi:10.1029/2004GL020670, 2004.

Schoof, C.: Ice sheet grounding line dynamics: Steady states, stability, and hysteresis, Journal of Geophysical Research, 112, F03S28, doi:10.1029/2006JF000664, http://doi.wiley.com/10.1029/2006JF000664, 2007.

Sergienko, O. V.: Basal channels on ice shelves, Journal of Geophysical Research: Earth Surface, 118, 1342–1355, 2013.

Shean, D. E., Christianson, K., Larson, K. M., Ligtenberg, S. R., Joughin, I. R., Smith, B. E., and Stevens, C. M.: In situ GPS records of surface mass balance and ocean-induced basal melt for Pine Island Glacier, Antarctica, The Cryosphere Discussions, pp. 1–30, doi:10.5194/tc-2016-288, http://www.the-cryosphere-discuss.net/tc-2016-288/, 2017.

Stanton, T. P., Shaw, W. J., Truffer, M., Corr, H. F. J., Peters, L. E., Riverman, K. L., Bindschadler, R., Holland, D. M., and Anandakrishnan, S.: Channelized ice melting in the ocean boundary layer beneath Pine Island Glacier, Antarctica, Science, 341, 1236–1239, doi:10.1126/science.1239373, http://www.ncbi.nlm.nih.gov/pubmed/24031016, 2013.

Tsai, V. C., Stewart, A. L., and Thompson, A. F.: Marine ice-sheet profiles and stability under Coulomb basal conditions, Journal of Glaciology, 61, 205–215, doi:10.3189/2015JoG14J221, http://www.ingentaconnect.com/content/igsoc/jog/2015/00000061/00000226/art00001, 2015.

Vaughan, D. G., Corr, H. F. J., Bindschadler, R. A., Dutrieux, P., Gudmundsson, G. H., Jenkins, A., Newman, T., Vornberger, P., and Wingham, D. J.: Subglacial melt channels and fracture in the floating part of Pine Island Glacier, Antarctica, Journal of Geophysical Research, 117, doi:10.1029/2012jf002360, http://dx.doi.org/10.1029/2012JF002360, 2012.

Wilson, N., Straneo, F., and Heimbach, P.: Submarine melt rates and mass balance for Greenland's remaining ice tongues, The Cryosphere Discussions, pp. 1–17, doi:10.5194/tc-2017-99, https://www.the-cryosphere-discuss.net/tc-2017-99/, 2017.

Wouters, B., Martin-Español, a., Helm, V., Flament, T., van Wessem, J. M., Ligtenberg, S. R. M., van den Broeke, M. R., and Bamber, J. L.: Dynamic thinning of glaciers on the Southern Antarctic Peninsula, Science, 348, 899–903, doi:10.1126/science.aaa5727, http://www.sciencemag.org/content/348/6237/899.abstract, 2015.

1 TanDEM-X frames

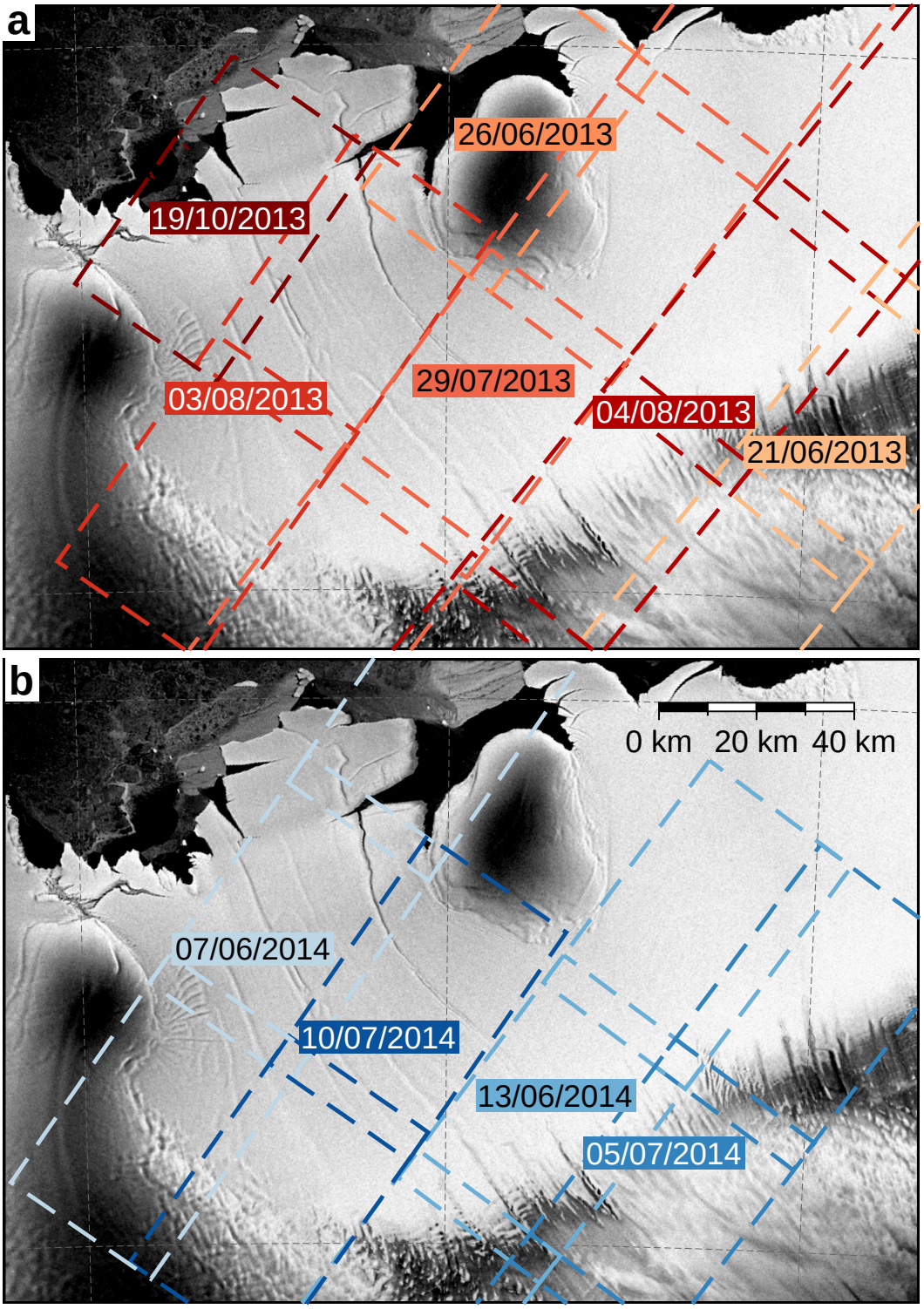

Figure S1: Frame location and dates of the TanDEM-X scenes from 2013 (a) and 2014 (b). The same color is used to represent different scenes acquired on the same day and satellite path tgat have been concatenated together with a linear taper and subsequently treated as one scene in our study (Sect. 2)

2 Gaussian filtering of TanDEM-X

Comparison between the GNSS profile from Drews (2015) and 2013 TanDEM-X DEM. Filtering the TanDEM-X elevations with a gaussian filter with a standard deviation of 7 pixels minimizes the the mean and standard deviation of the difference between the GNSS and TanDEM-X elevations: which are -0.41±0.38 m and -0.41±0.64 m for the filtered and unfiltered case, respectively.

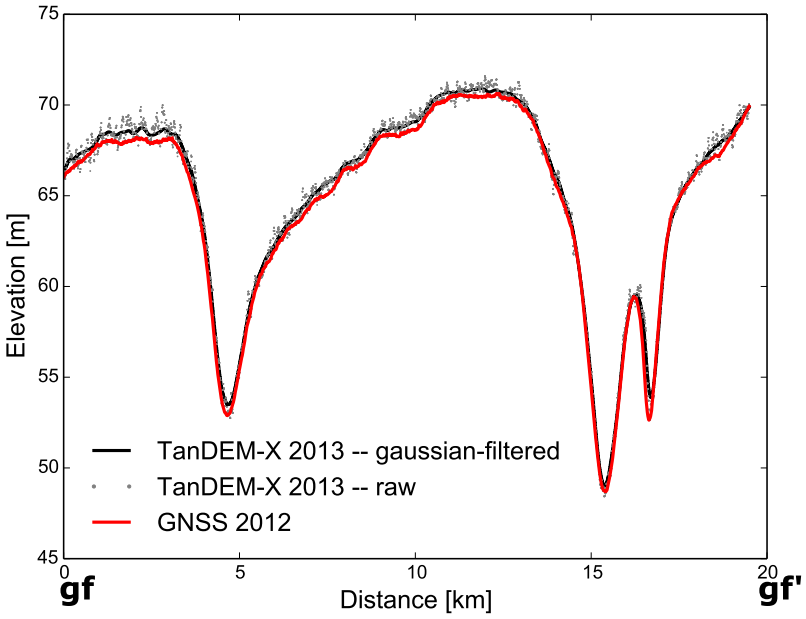

Figure S2: Comparison of unfiltered (raw) TanDEM-X 2013 , Gaussian-filtered TanDEM-X 2013 ($\sigma = 7$) and 2012 GNSS elevations. The profile gf-gf' is shown in Fig. 1. The Gaussian-filtering is discussed in Sect. 2.4.

3 TanDEM-X validation

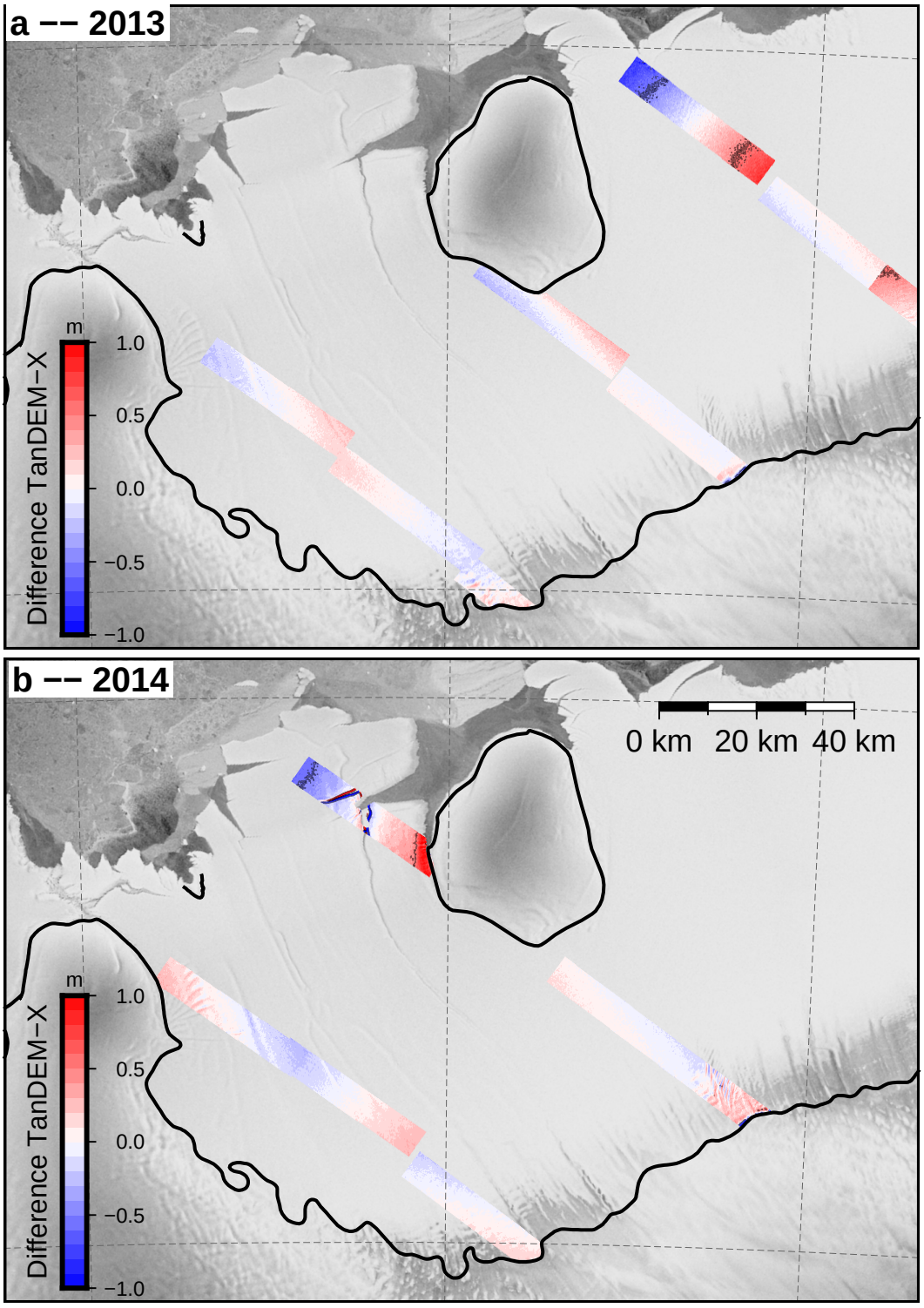

Figure S3: Elevation difference in the overlapping areas of consecutive (filtered) TanDEM-X scenes acquired the same day. The -0.5 and 0.5 contour lines have been added. This figure is discussed in Sect. 2.4 and 4.1

References

Drews, R.: Evolution of ice-shelf channels in Antarctic ice shelves, The Cryosphere, 9, 1169–1181, doi:doi: 10.5194/tc-9-1169-2015, 2015.